State of the Global Climate 2021

Key Messages

Atmospheric concentrations of the major greenhouse gases, carbon dioxide, methane and nitrous oxide, continued to increase in 2020 and 2021. The growth rate of all three greenhouse gases in 2020 was above the average for the last decade despite a 5.6% drop in fossil fuel CO_2 emissions in 2020 due to restrictions related to the COVID-19 pandemic.

Global mean temperature in 2021 (January to September) is around 1.08 ±0.13 °C above the 1850-1900 pre-industrial average and the year is likely to be between the 5th and 7th warmest year on record. 2021 is cooler than recent years owing to La Niña conditions early in the year.

The rate of global sea level rise has increased since satellite altimeter measurements began in 1993, reaching 4.4 mm/yr between 2013 and 2021. Global mean sea level reached a new record high in 2021.

Ocean heat content reached new record highs in 2019 and then 2020, the latest year for which a comprehensive analysis is available. Ocean warming rates show a particularly strong increase in the past two decades.

Changes in the global cryosphere in 2021 were consistent with recent multi-decadal trends, with below-normal Northern Hemisphere spring snow cover and end-of-summer Arctic sea ice area, negative mass balances on mountain glaciers and the Greenland and Antarctic Ice Sheets, and near-normal Antarctic sea ice cover.

The summer heat wave in western North America took a toll on the region's mountain glaciers, with exceptional mass losses in the Cascade, southern Coast, and Rocky Mountains. Mass loss at some glaciers in southwestern British Columbia was the greatest in the instrumental record (1965-2021).

Greenland experienced an exceptional mid-August melt event which included temperatures above 0 °C and rainfall at Summit Station, the highest point on the ice sheet. This is the first time that rain has been observed at Summit, and marks the third time in the last nine years that the Summit has experienced melting conditions. Ice core records indicate that only one such melt event occurred in the 20th century.

Exceptional heatwaves affected western North America on several occasions during June and July. Lytton, in south-central British Columbia, reached 49.6 °C on 29 June, breaking the previous Canadian national record by 4.6 °C. 569 heat-related deaths were reported in British Columbia alone between 20 June and 29 July.

Death Valley, California reached 54.4 °C on 9 July, equalling a similar 2020 value as the highest recorded in the world since at least the 1930s.

Extreme heat affected the broader Mediterranean region on several occasions during the second half of the Northern Hemisphere summer. The most exceptional heat was in the second week of August. On 11 August, an agrometeorological station near Syracuse in Sicily reached 48.8 °C, a provisional European record.

The most significant hurricane of the North Atlantic season was Ida. Ida made landfall in Louisiana on 29 August with sustained 1-minute winds of 240 km/h, the equal-strongest landfall on record for the state, with major wind damage and storm surge inundation. The system continued on a northeast track over land with significant flooding, especially in the New York City area. In total, 72 direct and 43 indirect deaths were attributed to Ida in the United States and Venezuela, with economic losses in the United States estimated at US$63.8 billion.

Extreme rainfall hit Henan Province of China from 17 to 21 July. On 20 July, the city of Zhengzhou received 201.9 mm of rainfall in one hour (a Chinese national record), 382 mm in 6 hours, and 720 mm for the event as a whole, more than its annual average. The city experienced extreme flash flooding with many buildings, roads and subways inundated. 302 deaths were attributed to the flooding, and economic losses of US$17.7 billion were reported.

Western Europe experienced some of its most severe flooding on record in mid-July. The worst-affected area was western Germany and eastern Belgium, where 100 to 150 mm fell over a wide area on 14-15 July over wet ground. The highest daily rainfall was 162.4 mm at Wipperfürth-Gardenau (Germany). Numerous rivers experienced extreme flooding, with several towns inundated, and there were also several landslides. 179 deaths were reported in Germany and 36 in Belgium, with economic losses in Germany exceeding US$20 billion.

Foreword

TBD

Global Climate Indicators

Global climate indicators[1] provide a broad view of climate change at a global scale, encompassing the composition of the atmosphere, energy changes largely caused by the accumulation of greenhouse gases, and the response of the land, ocean, and ice. These indicators are closely inter-related. For example, the rise in CO_2 and other greenhouse gases in the atmosphere leads to warming of the atmosphere and ocean. Warming of the ocean leads in turn to rising sea levels, which is added to by the melting of ice on land in response to increasing atmospheric temperatures. The global indicators draw on a wide range of data sets that are listed at the end of the report and show a consistent picture of a warming world.

The connections between global climate indicators and the Sustainable Development Goals were highlighted in "Climate Indicators and Sustainable Development: Demonstrating the Interconnections"[2]. The report demonstrates the linkages and feedback loops amongst the key climate indicators as a physical system and the resulting cascading risks to nearly all of the 17 Sustainable Development Goals, including those affecting environmental, social, and economic systems. Monitoring the global climate indicators, as well as their related risks and impacts, is therefore of critical importance for achieving the Sustainable Development Goals by 2030.

Baselines

Baselines are fixed periods, usually spanning one or more decades, that are used as a fixed point against which current conditions can be compared. A variety of baselines are used in this report and these are specified in the text and figures where appropriate.

Where possible the WMO climatological standard normal, 1981-2010, is used as a baseline for consistent reporting[3]. For some indicators however, it is not possible to use this baseline due to a lack of measurement during the whole period or because a longer period is needed to calculate representative statistics.

[1] https://journals.ametsoc.org/view/journals/bams/102/1/BAMS-D-19-0196.1.xml
[2] https://library.wmo.int/index.php?lvl=notice_display&id=21953
[3] 1981-2010 is used in preference to 1991-2020 for consistency with climate reports from WMO members not all of whom have yet transitioned to using the more recent period.

There are two notable exceptions. Firstly, for global mean temperature, a baseline of 1850-1900 is used. This is the baseline used in recent IPCC reports (AR6 WG1[4], SR15[5]) as a reference period for pre-industrial temperatures and is relevant for understanding progress relative to the long term goal of the Paris Agreement. For more details of how this is calculated see Global Temperature data. Secondly, for greenhouse gases, atmospheric concentrations can be estimated much further back in time, using gas bubbles trapped in ice cores. The year 1750 is used in this report to represent pre-industrial greenhouse gas concentrations.

Greenhouse gases

Atmospheric concentrations of greenhouse gases reflect a balance between emissions from human activities, natural sources and sinks in the biosphere and ocean. Increasing levels of greenhouse gases in the atmosphere due to human activities are the major driver of climate change since the mid-20th century. Global average mole fractions of greenhouse gases are calculated from in situ observations made at multiple sites in the Global Atmosphere Watch (GAW) Programme of WMO and partner networks.

In 2020, greenhouse gas concentrations reached new highs (Figure 1), with globally averaged surface mole fractions for carbon dioxide (CO_2) at 413.2 ± 0.2 parts per million (ppm), methane (CH_4) at 1889 ± 2 parts per billion (ppb) and nitrous oxide (N_2O) at 333.2 ± 0.1 ppb, respectively, 149%, 262% and 123% of pre-industrial (1750) levels. The increase in CO_2 from 2019 to 2020 was slightly lower than that observed from 2018 to 2019, but higher than the average annual growth rate over the last decade. This is despite the approximately 5.6% drop in fossil fuel CO_2 emissions in 2020 due to restrictions related to the COVID-19 pandemic[6]. For CH_4 and N_2O, the increase from 2019 to 2020 was higher than that observed from 2018 to 2019 and also higher than the average annual growth rate over the last decade.

Real-time data from specific locations, including Mauna Loa (Hawaii) and Cape Grim (Tasmania) indicate that levels of CO_2, CH_4 and N_2O continued to increase in 2021.

Atmospheric methane increase is an issue for concern because it is not only a powerful greenhouse gas but it also has, as a precursor of tropospheric ozone, implications for human health, agriculture and ecosystems[7]. The mean annual increase of CH_4 decreased from approximately 12 ppb yr^{-1} during the late 1980s to near zero between 1999 and 2006. Since 2007, atmospheric CH_4 has been increasing, and in 2020 it increased by 11 ppb over 2019 levels. Studies using GAW CH_4 measurements indicate that increased CH_4 emissions from wetlands in the tropics and from anthropogenic sources at the mid-latitudes of the Northern Hemisphere are the likely causes of this recent increase[8]. These studies also have pointed to the short-term climate benefits and cost-effectiveness of mitigating CH_4 emissions. Such mitigation measures were presented in the United Nations Environment Programme (UNEP) methane assessment[7] and address major emitting sectors, namely oil and gas, agriculture and waste management.

[4] AR6 Climate Change 2021: The Physical Science Basis https://www.ipcc.ch/report/ar6/wg1/
[5] IPCC Special Report: Global Warming of 1.5 °C https://www.ipcc.ch/sr15/
[6] https://public.wmo.int/en/resources/united_in_science https://library.wmo.int/index.php?lvl=notice_display&id=21946
[7] https://www.unep.org/resources/report/global-methane-assessment-benefits-and-costs-mitigating-methane-emissions
[8] Nisbet, E.G., M.R. Manning et al., 2019: Very strong atmospheric methane growth in the 4 years 2014–2017: Implications for the Paris Agreement. Global Biogeochemical Cycles, 33, 318–342, https://doi.org/10.1029/2018GB006009

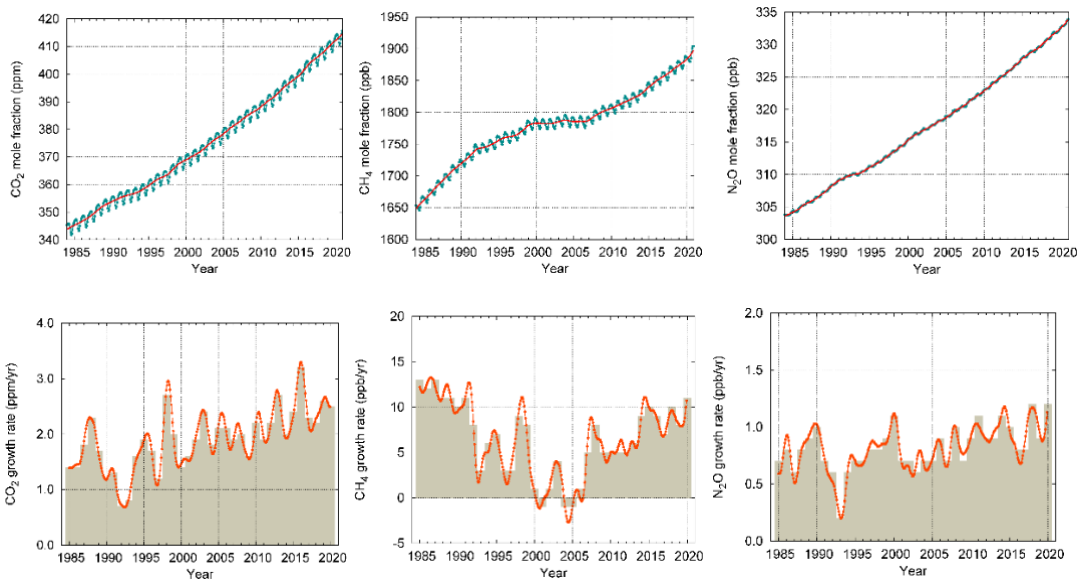

Figure 1: Top row: Globally averaged mole fraction (measure of concentration), from 1984 to 2020, of CO_2 in parts per million (left), CH_4 in parts per billion (centre) and N_2O in parts per billion (right). The red line is the monthly mean mole fraction with the seasonal variations removed; the blue dots and line show the monthly averages. Bottom row: the growth rates representing increases in successive annual means of mole fractions for CO_2 in parts per million per year are shown as grey columns (left), CH_4 in parts per billion per year (centre) and N_2O in parts per billion per year (right) (Source: WMO Global Atmosphere Watch).

Temperature

The global mean temperature for 2021 (based on data from January to September) was 1.08 ± 0.13°C above the 1850-1900 average (Figure 2). Currently, year-to-date averages from all data sets used in the analysis would place 2021 as the 6th (NOAAGlobalTemp) or 7th (all others) warmest year on record globally. However, three months of the year remain, and the ranking is liable to change. It is nevertheless likely that 2021 will be between the 5th and 7th warmest year on record and therefore likely that the most recent seven years, 2015 to 2021, will be the seven warmest years on record.

2021 is cooler than recent years due to the influence of a moderate La Niña at the start of the year (see Drivers of short-term variability). La Niña has a temporary cooling effect on the global mean temperature, which is strongest in the year following an event. Aside from the weak La Niña of 2018, the last significant La Niña event was in 2011. 2021 is around 0.18 to 0.26 °C warmer than 2011. As the 2020-21 La Niña has waned, monthly global temperatures have increased. However, conditions have approached La Niña thresholds again as of October. The year 2016, which started during a strong El Niño, remains the warmest year on record in most of the data sets surveyed.

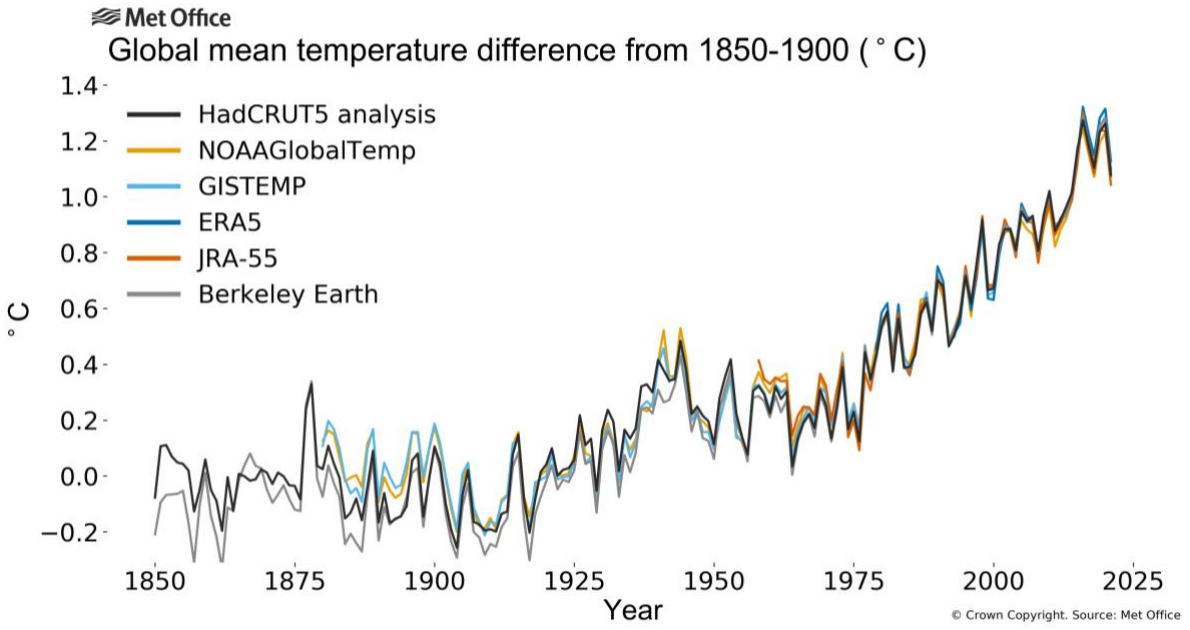

Figure 2: Global annual mean temperature difference from preindustrial conditions (1850–1900) for six global temperature data sets. For details of the datasets and processing see Data sets and methods.

The calculation of global temperature anomalies relative to the 1850-1900 baseline has been updated from previous State of the Global Climate reports. The new method uses the assessment of temperature change and its uncertainties from the IPCC Sixth Assessment Report (AR6) as a foundation for estimating changes since 1850-1900. Details are given in the section on Global Temperature data.

The Paris Agreement[9] aims to "*strengthen the global response to the threat of climate change, in the context of sustainable development and efforts to eradicate poverty, including by … Holding the increase in the global average temperature to well below 2°C above pre-industrial levels and pursuing efforts to limit the temperature increase to 1.5°C above pre-industrial levels, recognizing that this would significantly reduce the risks and impacts of climate change*".

Assessments of changes in climatological averages refer to long-term changes, in this case in the global mean temperature, and not to the temperature of a single year. In IPCC AR6 WG1 SPM, long-term change was assessed using a 20-year average. For the period, 2001-2020 the average was estimated[10] to be 0.99 [0.84-1.10] °C. The provisional 20-year average for the period 2002-2021, based on the average of the six data sets, was 1.01 ± 0.12 °C above the 1850-1900 average.

Near surface air temperatures for the first nine months of 2021 (Figure 3) were above the 1981-2010 average across a broad swath of North America and Greenland, northern and tropical Africa, the Middle East and southern Asia. Areas with below average temperatures included parts of northern Asia, Australia, southern Africa, northwest North America, and the southern central United States. The imprint of La Niña can clearly be seen in the tropical Pacific. Cooler conditions in southern Africa, India, and eastern Australia are characteristic of La Niña. The cooler-than-average area in northern Asia stands in contrast to 2020 which saw exceptionally high temperatures in the region, this is

[9] https://unfccc.int/sites/default/files/english_paris_agreement.pdf
[10] IPCC AR6 WG1 Summary for Policymakers A.1.2. The IPCC average was based on four data sets: HadCRUT5, NOAAGlobalTemp interim, Berkeley Earth and Kadow et al.

partly associated with the different phases of the Arctic Oscillation in early 2020 (strongly positive) and early 2021 (strongly negative, see the section on AO Arctic Oscillation).

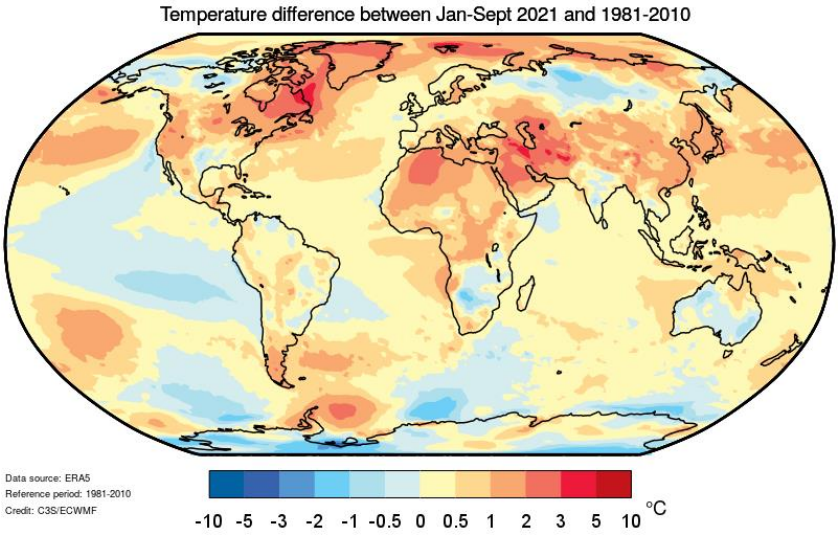

Figure 3: Near-surface air temperature differences from the 1981-2010 average for January to September 2021. Data are from the ERA5 reanalysis product. Source: Copernicus Climate Change Service/ECMWF

Ocean

Most of the excess energy that accumulates in the Earth system due to increasing concentrations of greenhouse gases is taken up by the ocean. The added energy warms the ocean, and the consequent thermal expansion of the water leads to sea level rise, which is added to by melting land ice. The surface layers of the ocean have warmed more rapidly than the interior, which can be seen in the rise of global mean sea-surface temperature and also in the increased incidence of marine heatwaves. As the concentration of CO_2 in the atmosphere increases, so too does the concentration of CO_2 in the ocean. This affects ocean chemistry, lowering the average pH of the water, a process known as ocean acidification. All these changes have a broad range of impacts in the ocean and coastal areas. Note that with reporting delays, the most recent data for some of these indicators are from 2020.

Ocean heat content

Increasing human emissions of CO_2 and other greenhouse gases cause a positive radiative imbalance at the top of the atmosphere – the Earth Energy Imbalance (EEI) – leading to an accumulation of energy in the form of heat in the Earth system which is driving global warming[11,12,13]. Around 90% of this accumulated heat in the Earth system is stored in the ocean, which is measured through Ocean Heat Content (OHC). A positive EEI signals that the Earth's climate system is still responding to the current forcing[14] and that more warming will occur even if the forcing does not increase further[15]. This in turn is reflected in a continued increase of ocean heat content. IPCC AR6 Working Group 1 (WG1) concluded that it is unequivocal that human influence has warmed the atmosphere, ocean

[11]Hansen, J. et al. (2011). Earth's energy imbalance and implications. Atmospheric Chemistry and Physics. https://doi.org/10.5194/acp-11-13421-2011
[12] Rhein, M. et al. 2013. Climate change 2013: The physical science basis.
[13] von Schuckmann, K. et al. (2016). An imperative to monitor Earth's energy imbalance. In Nature Climate Change. https://doi.org/10.1038/nclimate2876
[14] Hansen, J. et al. (2005). Earth's Energy Imbalance: Confirmation and Implications. Science, 308(5727), 1431 LP – 1435. https://doi.org/10.1126/science.1110252
[15] Hansen, J. et al. (2017). Young people's burden: requirement of negative CO2 emissions. Earth Syst. Dynam., 8(3), 577–616. https://doi.org/10.5194/esd-8-577-2017

and land, and that it is extremely likely that human influence was the main driver of the ocean heat increase observed since the 1970s[16].

Historical measurements of subsurface temperature back to the 1940s mostly rely on shipboard measurement systems, which constrains the availability of subsurface temperature observations at a global scale and at depth[17]. With the deployment of the Argo network of autonomous profiling floats, which first achieved near-global coverage in 2006, it is now possible to routinely measure OHC changes down to a depth of 2000m[18,19].

Various research groups have developed estimates of global OHC, and all results show continued ocean warming (Figure 4). Differences between the estimates at annual to decadal scale arise from the various statistical treatments of data gaps, the choice of climatology and the approach used to account for instrumental biases[20,21]. A concerted effort has been established to provide an international view on the global evolution of ocean warming[22] up to the year 2020.

The upper 2000m depth of the ocean continued to warm in 2019 reaching a new record high, and it is expected that it will continue to warm in the future[23,24]. A preliminary analysis based on seven global data sets suggests that 2020 exceeded that record (Figure 4). All data sets agree that ocean warming rates show a particularly strong increase in the past two decades. Ocean warming rates for the 0-2000m depth layer reached 1.0 (0.6) ± 0.1 Wm^{-2} over the period 2006-2020 (1971-2020). For comparison, the values for the upper 700m depth amount to 0.6 (0.4) ± 0.1 Wm^{-2} over the period 2006-2020 (1971-2020). Below 2000m depth, the ocean also warmed albeit at the lower rate of 0.07 ± 0.04 Wm^{-2} from 1991-2018[25].

[16] IPCC, 2021: Summary for Policymakers. In: Climate Change 2021: The Physical Science Basis. Contribution of Working Group I to the Sixth Assessment Report of the Intergovernmental Panel on Climate Change [MassonDelmotte, V., P. Zhai, A. Pirani, S.L. Connors, C. Péan, S. Berger, N. Caud, Y. Chen, L. Goldfarb, M.I. Gomis, M. Huang, K. Leitzell, E. Lonnoy, J.B.R. Matthews, T.K. Maycock, T. Waterfield, O. Yelekçi, R. Yu, and B. Zhou (eds.)]. Cambridge University Press. In Press.

[17] Abraham, J. P. et al. (2013). A review of global ocean temperature observations: Implications for ocean heat content estimates and climate change. Reviews of Geophysics, 51(3), 450–483. https://doi.org/10.1002/rog.20022

[18] Riser, S. C. et al. (2016). Fifteen years of ocean observations with the global Argo array. Nature Climate Change, 6(2), 145–153. https://doi.org/10.1038/nclimate2872

[19] Roemmich, D. et al. (2019). On the Future of Argo: A Global, Full-Depth, Multi-Disciplinary Array. In Frontiers in Marine Science (Vol. 6, p. 439). https://www.frontiersin.org/article/10.3389/fmars.2019.00439

[20] Boyer, T. et al. (2016). Sensitivity of Global Upper-Ocean Heat Content Estimates to Mapping Methods, XBT Bias Corrections, and Baseline Climatologies. Journal of Climate, 29(13), 4817–4842. https://doi.org/10.1175/JCLI-D-15-0801.1

[21] von Schuckmann, K. et al. (2016). An imperative to monitor Earth's energy imbalance. In Nature Climate Change. https://doi.org/10.1038/nclimate2876

[22] von Schuckmann, K. et al. (2020). Heat stored in the Earth system: Where does the energy go? The GCOS Earth heat inventory team. Earth Syst. Sci. Data Discuss., 2020, 1–45. https://doi.org/10.5194/essd-2019-255

[23] IPCC, 2019: Summary for Policymakers. In: IPCC Special Report on the Ocean and Cryosphere in a Changing Climate [H.-O. Pörtner, D.C. Roberts, V. Masson-Delmotte, P. Zhai, M. Tignor, E. Poloczanska, K. Mintenbeck, A. Alegría, M. Nicolai, A. Okem, J. Petzold, B. Rama, N.M. Weyer (eds.)]. In press.

[24] IPCC, 2021: Summary for Policymakers

[25] Update from Purkey, S. G., and G. C. Johnson, 2010: Warming of Global Abyssal and Deep Southern Ocean Waters between the 1990s and 2000s: Contributions to Global Heat and Sea Level Rise Budgets. J. Climate, 23, 6336–6351, https://doi.org/10.1175/2010JCLI3682.1

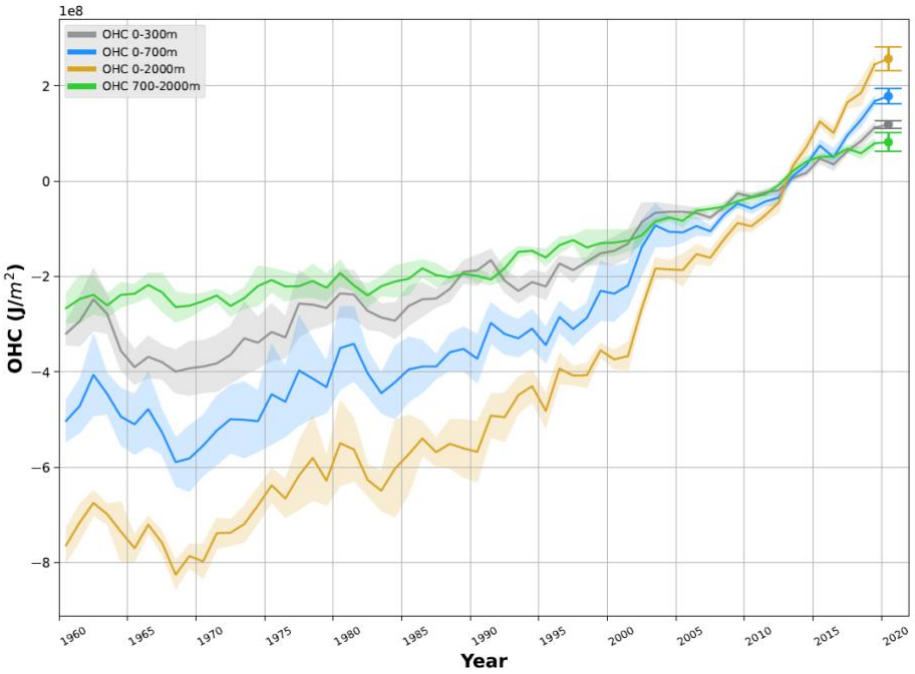

Figure 4: 1960-2020 ensemble mean time series and ensemble standard deviation (2-standard deviations, shaded) of global ocean heat content (OHC) anomalies relative to the 2005-2017 average for the 0-300m (grey), 0-700m (blue), 0-2000m (yellow) and 700-2000m depth layer (green). The ensemble mean is an outcome of a concerted international effort, and all products used are listed in von Schuckmann et al., 2020. Note that values are given for the ocean surface area between 60°S-60°N, and limited to the 300m bathymetry of each product. Updated from von Schuckmann et al. (2020). The ensemble mean OHC (0-2000m) anomaly (relative to the 1993-2020 average) has been added as a cross, together with its ensemble spread, and is based on the 7 products listed in Ocean heat content data.

Sea level

Global mean sea level (GMSL) is one of the key global climate indicators. It integrates changes occurring in many components of the climate system; on interannual to multidecadal time scales, GMSL changes result from ocean warming via thermal expansion of sea water, melting of land ice and exchange of water with water bodies on land. Measured since the early 1990s by high precision altimeter satellites, the mean GMSL rate was 2.1 mm yr^{-1} between 1993 and 2002 and 4.4 mm yr^{-1} between 2013 and 2021, an increase by a factor of 2 between the periods, mostly due to the accelerated loss of ice mass from the ice sheets[26]. In 2021, GMSL reached a new record high. Compared to previous El Niño and La Niña years (e.g., in 1997-1998, 2010-2011, 2015-2016), during which the GMSL displayed temporary positive or negative anomalies of several millimetres, 2021 was marked by an increase of the GMSL that was close to the long-term trend (Figure 5).

[26] WCRP Global Sea Level Budget Group: Global sea-level budget 1993–present, Earth Syst. Sci. Data, 10, 1551–1590, https://doi.org/10.5194/essd-10-1551-2018, 2018.

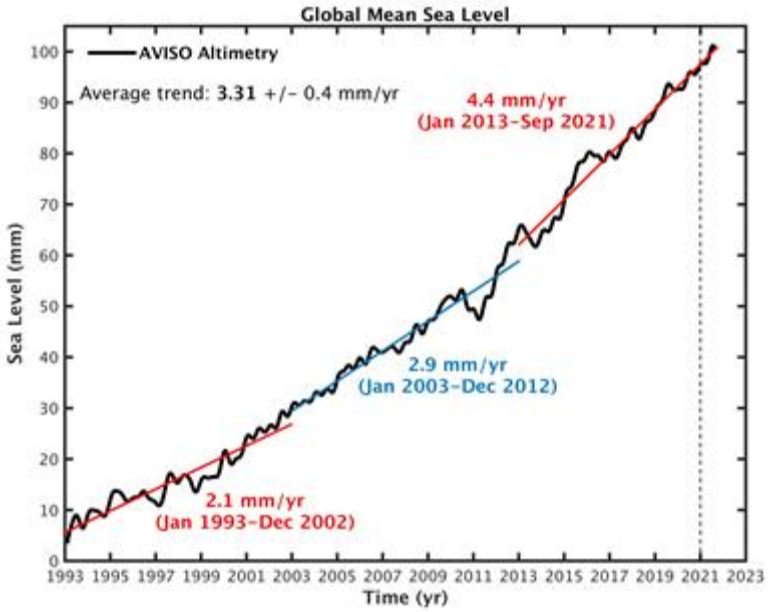

Figure 5: Global mean sea level evolution from January 1993 to September 2021 (black curve) based on high precision satellite altimetry. The coloured straight lines represent the average linear trend over 3 successive time spans (January 1993-December 2002; January 2003-December 2012; January 2013-September 2021). The thin vertical dashed line separates 2021 from previous years. Data source: AVISO altimetry (https://www.aviso.altimetry.fr)

Although sea level has risen almost everywhere since 1993, sea level has not risen equally everywhere. Regional patterns of sea level change are dominated by local changes in ocean heat content and salinity. Several regions continue to be affected by a rate of sea level rise substantially faster than the global mean (see Figure 6, which shows the difference between local and global sea level). This is particularly the case in the western tropical Pacific east of the Philippines and New Guinea, the southwest Pacific east of Australia and New Zealand, the north Pacific, the southwest Indian ocean east of Madagascar, and the south Atlantic. In other regions, local sea level has risen more slowly than the global mean e.g., around Greenland and south of Iceland, and in the Southern Ocean around Antarctica. The patterns of trends in sea level have only varied a little over the last 30 years of the altimetry era, and changes from one year to another are small.

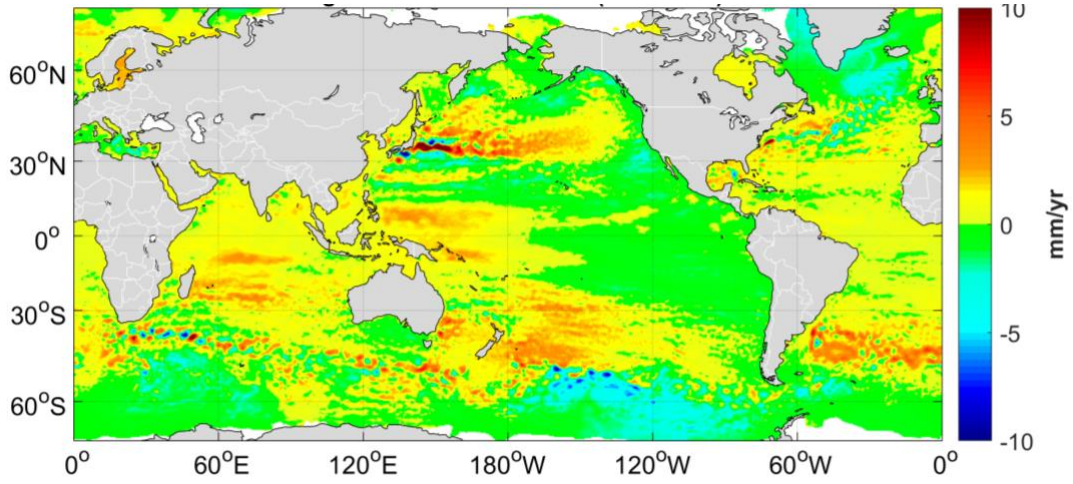

Figure 6: Regional trend patterns in sea level after the global mean trend has been removed, over 1993-2020 based on satellite altimetry. Unit: mm/yr. Data source: Copernicus Climate Change Service (https://climate.copernicus.eu). Note that the actual sea level has increased almost everywhere.

Marine heatwaves and cold spells

In analogy with heatwaves and cold spells on land, Marine Heat Waves (MHW) and Marine Cold Spells (MCS) are prolonged periods of extreme heat or cold that affect the near-surface layer of the ocean. They can have a range of consequences for marine life and dependent communities[27] and MHWs have become more frequent over the 20th Century. Satellite retrievals of sea-surface temperature are used to monitor MHWs and MCSs, categorized here as moderate, strong, severe, or extreme (for definitions, seeMarine heatwave and marine cold spell data).

Much of the ocean experienced at least one 'strong' MHW at some point in 2021 (to 14 October, Figure 7). MHWs were conspicuously absent in the eastern equatorial Pacific Ocean – linked to below average sea-surface temperatures associated with La Niña – and much of the Southern Ocean – one of the few areas in which MCSs are increasing in duration. The Laptev and Beaufort Seas experienced "severe" and "extreme" MHWs from January to April 2021. In 2021, almost all MCSs were 'moderate', except in areas of high variability such as the poleward extension of the Gulf Stream. The eastern equatorial Pacific Ocean experienced almost no MHWs in 2021 and was one of the few non-polar regions of the global ocean to see broad MCS coverage.

MHWs in 2021 (to 14 October) showed an average daily coverage of 13%, which is less than the record of 17% in 2016 and 16% in 2020. Nearly 25% of MHWs were classified as 'strong', another 25% as 'moderate', and 55% of the ocean surface experienced at least one MHW during 2021 (Figure 7c) – less than the record of 65% in 2016 and 63% in 2020.

The average daily coverage of the global ocean by MCSs in 2021 (to 14 October) was 3% (Figure 8b) – a lower value than the record high in 1982 (7%) and less than 2020 (4%). MCSs in 2021 were predominantly classified as 'moderate' (17%) and 'strong' (3%). In total, 22% of the ocean surface experienced at least one MCS during 2021 (Figure 8c), which is lower than 2020 (25%) and 1985 (63%).

[27] Smale, D. A., Wernberg, T., Oliver, E. C., Thomsen, M., Harvey, B. P., Straub, S. C., ... & Moore, P. J. (2019). Marine heatwaves threaten global biodiversity and the provision of ecosystem services. Nature Climate Change, 9(4), 306-312.

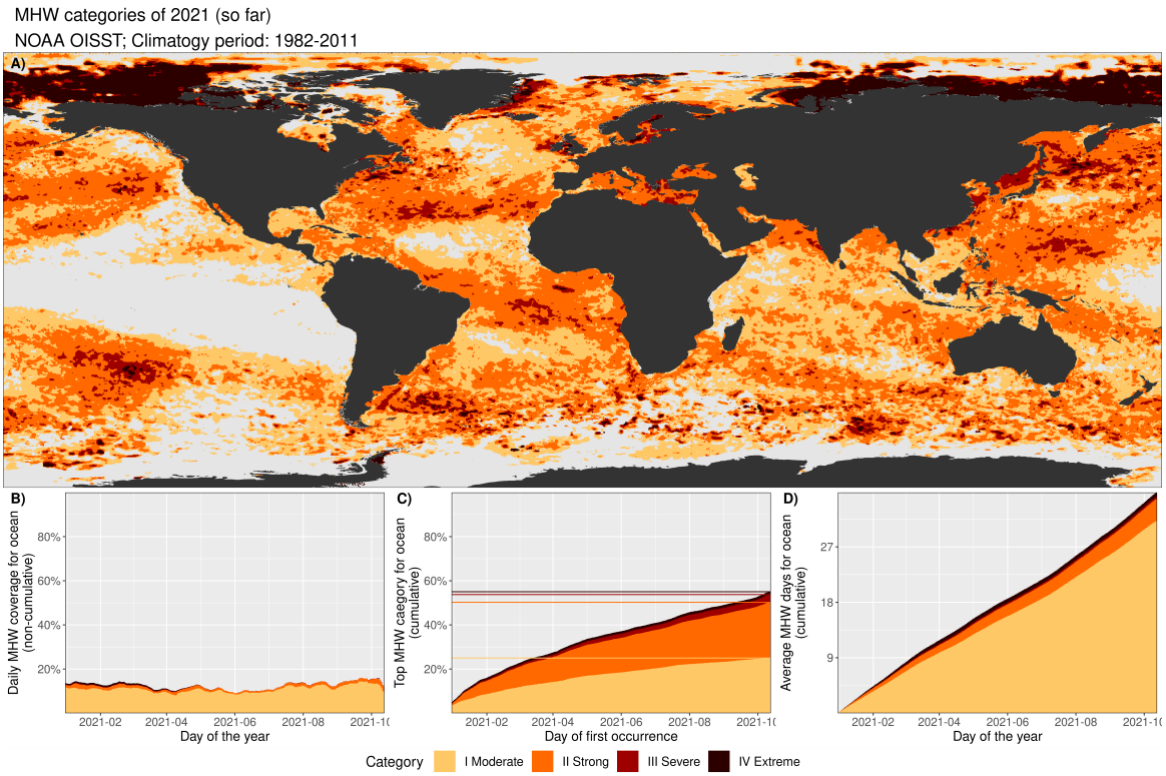

Figure 7: (a) Global map showing the highest MHW category (for definitions, see Marine heatwave and marine cold spell data) experienced at each pixel from 1 January to 14 October 2021 (reference period 1982–2011). Light grey indicates that no MHW occurred in a pixel over the entire year; (b) Stacked bar plot showing the percentage of the surface of the ocean experiencing an MHW on any given day of the year; (c) Stacked bar plot showing the cumulative percentage of the surface of the ocean that experienced an MHW over the year. Note: These values are based on when in the year a pixel first experienced its highest MHW category, so no pixel is counted twice. Horizontal lines in this figure show the final percentages for each category of MHW; (d) Stacked bar plot showing the cumulative number of MHW days averaged over the surface of the ocean. Note: This average is calculated by dividing the cumulative sum of MHW days per pixel weighted by the surface area of those pixels. Data are from NOAA OISST. Source: Robert Schlegel

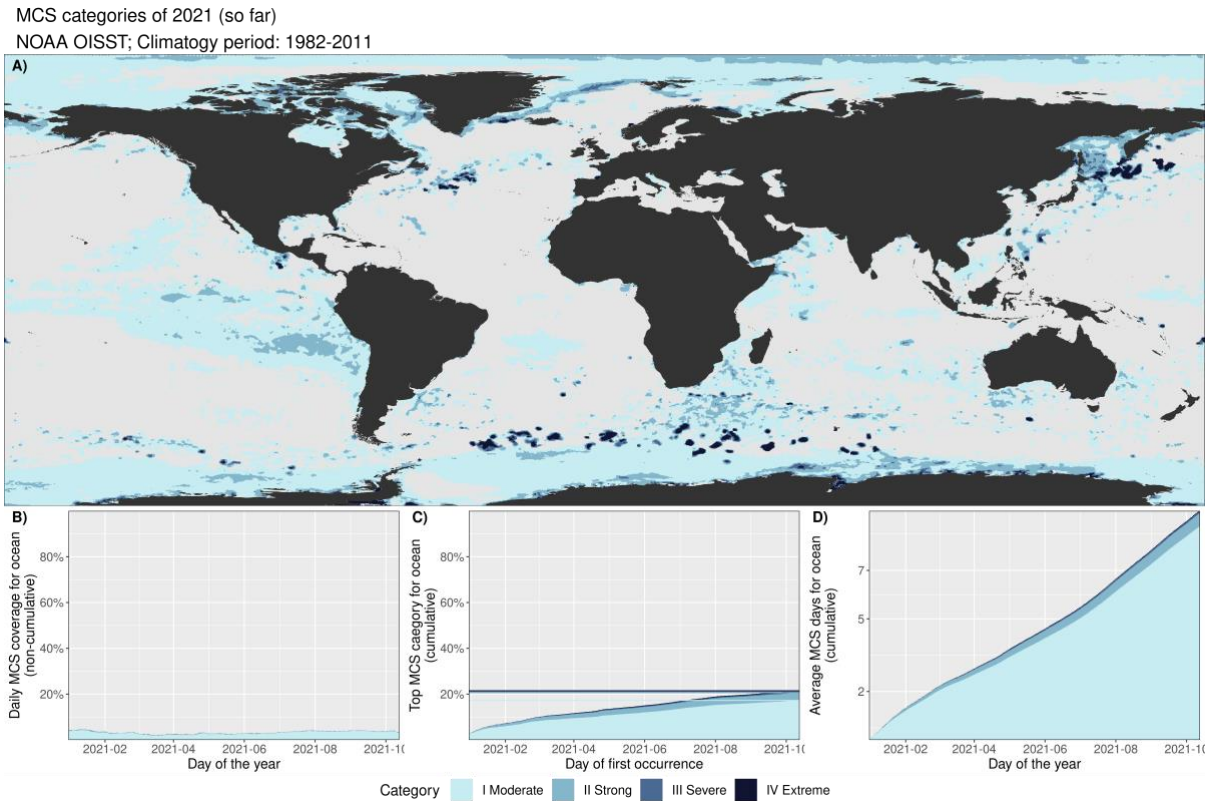

Figure 8: as for Figure 7 but showing Marine Cold Spells rather than Marine Heat Waves. Data are from NOAA OISST. Source: Robert Schlegel

Ocean acidification

The ocean absorbs around 23% of the annual emissions of anthropogenic CO_2 to the atmosphere[28,29], while this slows the rise of atmospheric concentration of CO_2[30] and the related warming, the costs to the ocean are high. CO_2 reacts with seawater and reduces the pH of the ocean[31], a process known as ocean acidification. The current global rate of ocean acidification (Figure 9) exceeds, by at least an order of magnitude, the rates inferred for the Paleocene-Eocene Thermal Maximum (PETM), which occurred around 56 million years ago and was associated with large perturbations of the global carbon cycle[32]. The IPCC AR6 concluded that "*there is* very high confidence *that open ocean surface pH is now the lowest it has been for at least 26 kyr and current rates of pH change are unprecedented since at least that time*". As the pH of the ocean decreases, its capacity to absorb CO_2 from the atmosphere also declines[33].

Ocean acidification threatens organisms and ecosystem services, and hence food security, tourism and coastal protection. Local and regional acidification is of great relevance to marine organisms and

[28] IPCC, 2019: IPCC Special Report on the Ocean and Cryosphere in a Changing Climate [H.-O. Pörtner, D.C. Roberts, V. Masson-Delmotte, P. Zhai, M. Tignor, E. Poloczanska, K. Mintenbeck, A. Alegría, M. Nicolai, A. Okem, J. Petzold, B. Rama, N.M. Weyer (eds.)].
[29] https://library.wmo.int/index.php?lvl=notice_display&id=21620
[30] Le Quéré, C., Andrew, R. M., Friedlingstein, P., Sitch, S., Pongratz, J., Manning, A. C., et al. (2018). Global carbon budget 2017. Earth Syst. Sci. Data 10, 405–448. doi: 10.5194/essd-10-405-2018
[31] IPCC, 2021: Climate Change 2021: The Physical Science Basis. Contribution of Working Group I to the Sixth Assessment Report of the Intergovernmental Panel on Climate Change [Masson-Delmotte, V., P. Zhai, A. Pirani, S.L. Connors, C. Péan, S. Berger, N. Caud, Y. Chen, L. Goldfarb, M.I. Gomis, M. Huang, K. Leitzell, E. Lonnoy, J.B.R. Matthews, T.K. Maycock, T. Waterfield, O. Yelekçi, R. Yu, and B. Zhou (eds.)]. Cambridge University Press. In Press.
[32] IPCC AR6 WG1 Chapter 2, section 2.3.3.5 Ocean pH
[33] Middelburg, J. J., Soetaert, K., &Hagens, M. (2020). Ocean alkalinity, buffering and biogeochemical processes. Reviews of Geophysics,58,e2019RG000681. https://doi.org/10.1029/2019RG000681

biological processes. However, there is high variability in coastal areas due to a range of factors affecting CO_2 levels.

National datasets of ocean acidification observations submitted towards the Sustainable Development Goal (SDG) 14.3 and the associated SDG Indicator 14.3.1 ("Average marine acidity (pH) measured at agreed suite of representative sampling stations",

Figure 10) highlight the need for sustained, repeated observation and measurement of ocean acidification along the coastlines and in the open ocean to improve understanding of its consequences, enable modelling and predictions of change and variability. While there are currently still gaps in the global coverage, capacity building efforts increase the capability of many nations to measure, manage and report ocean acidification data, as confirmed by the growing number of countries participating in data collection towards the SDG Indicator 14.3.1.

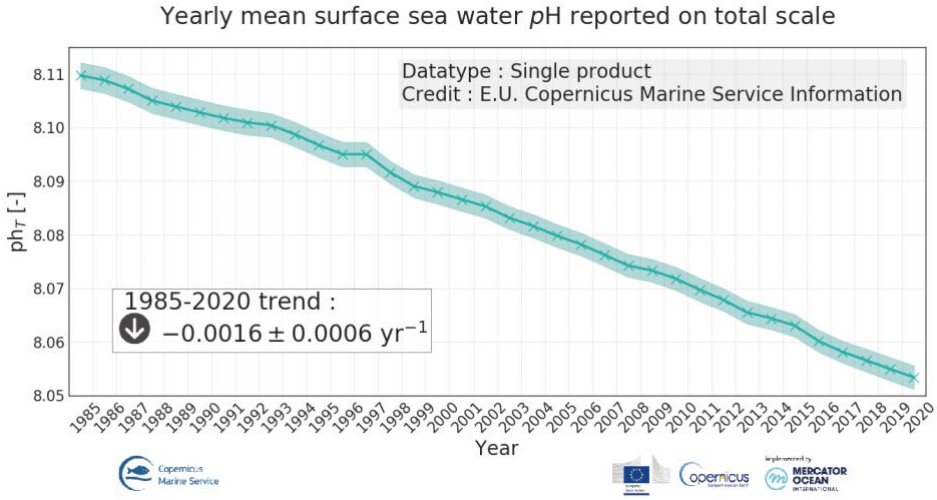

Figure 9: Global mean surface pH 1985 to 2020 from E.U. Copernicus Marine Service Information (blue). The shaded area indicates the estimated uncertainty.

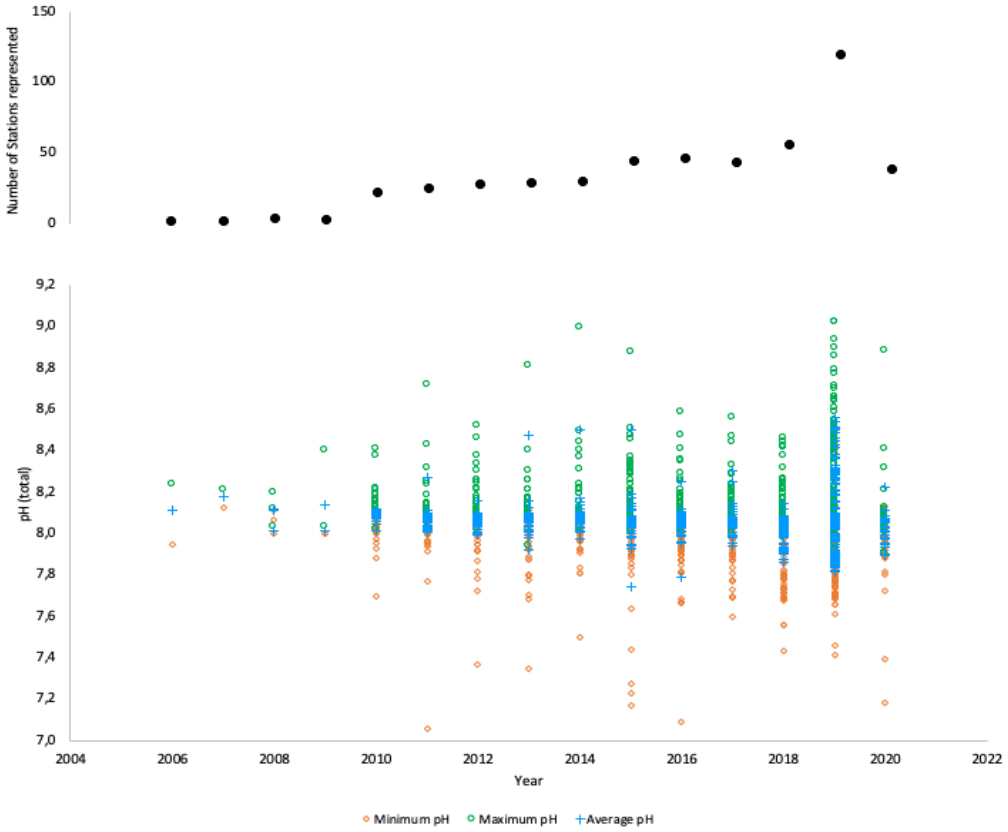

Figure 10: (left) Calculated surface pH values based on ocean acidification data submitted to the 14.3.1 data portal (http://oa.iode.org). Top panel: Black dots – number of stations represented per year. Bottom panel: Blue crosses – average annual pH reported from quality assured measurements; orange diamonds – annual minimum pH values reported for each station; green circles – annual maximum pH values reported for each station.

Cryosphere

The cryosphere comprises the frozen parts of the earth. This includes sea ice, glaciers, ice sheets, snow, and permafrost, all of which are covered in this report. Note that with reporting delays, the most recent data for some of these indicators are from 2020.

Sea ice

Arctic sea ice

The 2020-2021 Arctic winter saw anomalously high sea-level pressure over the central Arctic Ocean. The resulting anticyclonic wind pattern drove thicker multiyear ice into the Beaufort Sea[34]. The maximum Arctic sea-ice extent for the year was reached[35] on 21 March, at 14.8 million km^2. March 2021 was the 9th or 10th lowest extent on record (1979-2021), depending on the data source. For more details on the data sets used, see Sea ice.

Melt rates were close to the 1981-2010 average early in the melt season. However, sea-ice extent decreased very rapidly in June and early July in the Laptev Sea and East Greenland Sea regions. As a result, the Arctic-wide sea-ice extent was record low in the first half of July. The monthly July average was the 2nd to 4th lowest on record (tied with 2012 and 2019), with strong regional contrasts[36] (Figure 12). More ice than normal (1981-2010) was found in the Beaufort and Chukchi

[34] Mallett, R.D.C., Stroeve, J.C., Cornish, S.B. et al. (2021). Record winter winds in 2020/21 drove exceptional Arctic sea ice transport. Commun Earth Environ 2, 149 https://doi.org/10.1038/s43247-021-00221-8

[35] https://nsidc.org/arcticseaicenews/2021/03/arctic-sea-ice-reaches-uneventful-maximum

[36] https://climate.copernicus.eu/sea-ice-cover-july-2021

Seas, but the Siberian and European sectors (Laptev Sea and East Greenland Sea) had much less sea ice than normal. One exception was the Eastern Kara Sea, where some sea ice persisted for the whole season. Conditions shifted rapidly after July, with a sustained period of colder weather across the Arctic Ocean. This slowed the sea-ice melt and August 2021 ended-up with the 10th lowest extent on record, possibly also related to thicker multiyear ice in the Beaufort Sea that resisted melting.

Assisted by the August slowdown in melt, the minimum September extent was greater than in recent years but still well below the 1981-2010 average, representing the 12th lowest minimum ice extent in the 43-year satellite record (Figure 11). The 2021 minimum extent was observed[37] on 16 September at 4.72 million km^2 while the mean September ice extent was 4.92 million km^2, significantly below the 1981-2010 average. Sea-ice extent in the East Greenland Sea was a record low by a large margin.

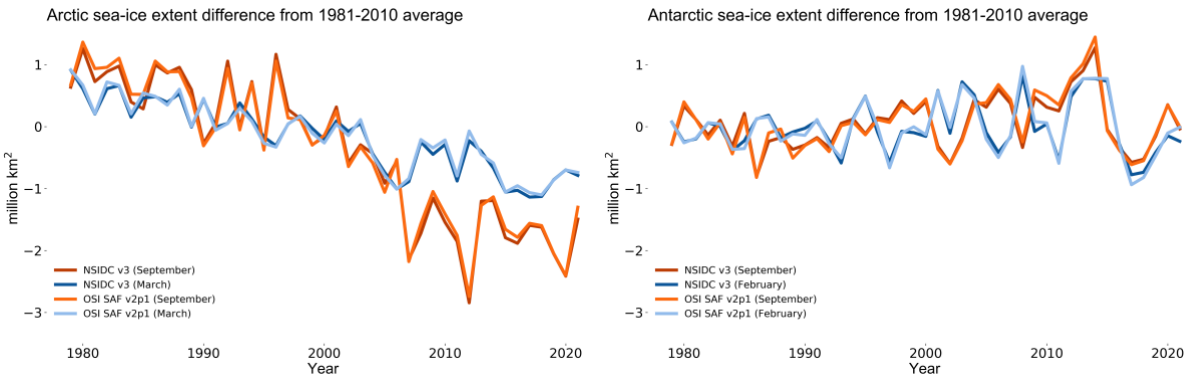

Figure 11: Sea-ice extent difference from the 1981–2010 average in the Arctic (left) and Antarctic (right) for the months with maximum ice cover (Arctic: March; Antarctic: September) and minimum ice cover (Arctic: September; Antarctic: February). Source: Data from EUMETSAT OSI SAF v2p1 and National Snow and Ice Data Centre (NSIDC) v3 (Fetterer et al., 2017) (see reference details in Sea-ice data).

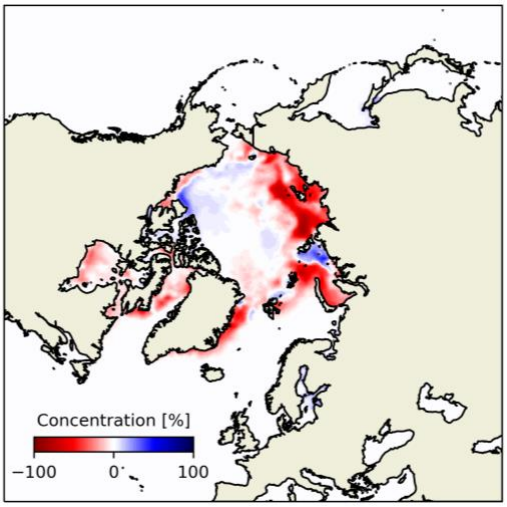

Figure 12: Arctic sea-ice concentration anomaly for July 2021 (difference from the 1981-2010 average). Red represents areas with less ice than normal, blue means more ice. Source: EUMETSAT OSI SAF data with research and development input from ESA CCI.

[37] https://nsidc.org/arcticseaicenews/2021/09/arctic-sea-ice-at-highest-minimum-since-2014

Antarctic sea ice

Sea-ice extent across the Southern Ocean during the first 9 months of 2021 was generally below the 1981–2010 mean, with a relatively low February minimum but near- average conditions during the summer melt season. There was an exceptionally early maximum ice extent at the end of August.

The minimum in the 2021 annual cycle occurred on 19 February, when sea ice covered 2.60 million km^2, the 15th lowest extent in the record (1979-present). The extent of ice at the annual minima began to increase in magnitude in the early 1990s, reaching a maximum of 3.68 million km^2 in 2013, before dropping sharply to 2.08 million km^2 in 2017, the lowest ice extent in the record. Since then, the extents at the annual minima have increased slowly. In February, most Antarctic sea ice is found in the Weddell Sea and therefore the sea-ice extents at the annual minima reflect regional changes in that area.

Antarctic sea ice reached its maximum annual extent of 18.80 million km^2 on 30 August 2021. This was close to the average magnitude in terms of extent and the 22nd largest in the 43 years of data. However, this was the 2nd earliest maximum, with only one other maximum having occurred in August (that of 2016). During July and August both the Amundsen Sea Low to the west of the Antarctic Peninsula and the Lazarev Sea Low close to the Greenwich Meridian were deeper than normal, leading to stronger than average offshore flow that led to positive sea ice anomalies in the Amundsen and Ross Seas, and between the northeast Weddell Sea and 90˚ E.

Glaciers

Glaciers are formed from snow that has compacted to form ice, which can deform and flow downhill to lower and warmer altitudes where it melts. If the glacier terminates in a lake or the ocean, ice loss also occurs through melting where ice and water meet or by calving of the glacier front to form icebergs. Glaciers are sensitive to changes in temperature, precipitation, and sunlight, as well as other factors such as changes in basal lubrication, warming ocean waters, or the loss of buttressing ice shelves.

Over the period 2000-2019, global glaciers and ice caps (excluding the Greenland and Antarctic Ice Sheets) experienced[38] an average mass loss of 267 ± 16 Gt yr^{-1}. Mass loss increased to 298 ± 24 Gt yr^{-1} from 2015-2019. Glaciers in several mid-latitude regions thinned at more than double the global average (0.52 ± 0.03 m yr^{-1}) from 2015-2019, e.g., -1.52 m yr^{-1} in New Zealand, -1.24 m yr^{-1} in Alaska, -1.11 m yr^{-1} in Central Europe, and -1.05 m yr^{-1} in western North America (not including Alaska).

According to the World Glacier Monitoring Service, in the hydrological year 2019-2020, the 40 or so glaciers with long-term observations experienced an average mass balance of -0.98 m water equivalent (m w.e[39]. Figure 13), less than in the record years 2018 and 2019, but still ranking as the 5th most negative mass balance year on record, for the period 1950-2020. Despite the global pandemic, mass balance observations were collected for most glacier monitoring sites worldwide, although some data gaps will be inevitable. Preliminary results for 2021 are only available for a few selected regions at this time, including for southwestern Canada and the Swiss Alps.

[38] Hugonnet, R., McNabb, R., Berthier, E., Menounos, B., Nuth, C., Girod, L., Farinotti, D., Huss, M., Dussaillant, I., Brun, F. and Kääb, A., 2021. Accelerated global glacier mass loss in the early twenty-first century. Nature, 592 (7856), 726-731.

[39] Metres water equivalent is the depth of water you would get if the lost ice were melted and spread across the surface area of the glacier.

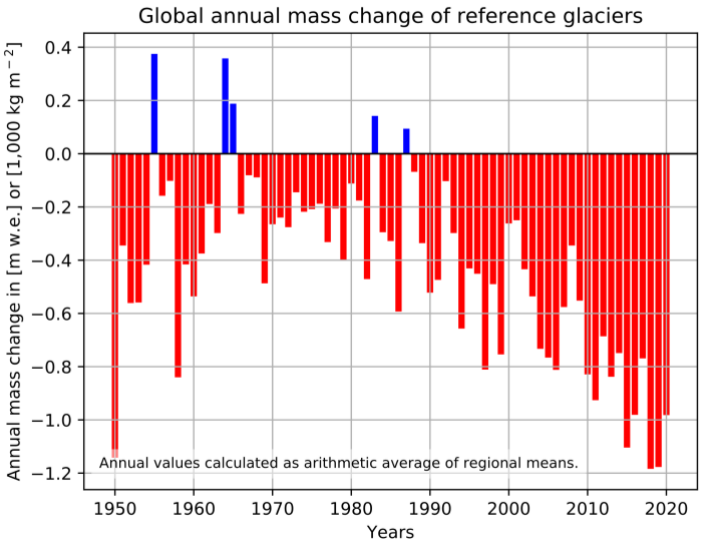

Figure 13: Global glacier mass balance, 1950-2020, from a subset of around 40 global reference glaciers. Units are m w.e. which is the depth of water that would be obtained from melting the lost ice and distributing it evenly across the glaciers. Data and image curated by the World Glacier Monitoring Service, http://www.wgms.ch.

Exceptional Glacier Mass Loss in Western Canada:

Mass loss from North American glaciers accelerated over the last two decades. Glacier mass loss in western North America increased from 53 ± 13 Gt yr^{-1} for the period 2000-2004 to 100 ± 17 Gt yr^{-1} for 2015-2019[38].

An exceptionally warm, dry summer in 2021 (see Heatwaves and wildfires) exacerbated mass loss for most glaciers in southern British Columbia, Alberta and the US Pacific Northwest. In the Coast Mountains of British Columbia, Place and Helm glaciers lost more mass during the period 2020-2021 than in any year since measurements began in 1965 (Figure 14a). In the Canadian Rocky Mountains, mass loss from Peyto Glacier was the second greatest since 1965, after the strong El Niño year of 1998 (Figure 14b). Repeat LiDAR surveys[40] indicate mass balances of -2.66, -3.30, and -1.95 m w.e. on Place, Helm, and Peyto glaciers, respectively. This represents roughly twice the mean regional rate of thinning from 2015-2019.

Little snow remained on most of the mountain glaciers in this region by mid-August, and many of these glaciers have lost their firn zone, where multi-year snow undergoes the transformation from snow to glacial ice. Particulate deposition – including soot and ash – from extensive regional wildfire activity in summer 2021 meant that the surfaces of the glaciers were unusually dark in July and August and absorbed more sunlight than usual, contributing to the extreme mass loss. Kokanee Glacier, British Columbia, lost 5-6% of its total volume in 2021, while Columbia Icefield, the largest icefield in the Rocky Mountains (210 km^2), lost about 0.34 Gt of ice (Figure 14c).

[40] Pelto, B. M., Menounos, B., and Marshall, S. J., 2019. Multi-year evaluation of airborne geodetic surveys to estimate seasonal mass balance, Columbia and Rocky Mountains, Canada. The Cryosphere, 13, 1709–1727, https://doi.org/10.5194/tc-13-1709-2019.

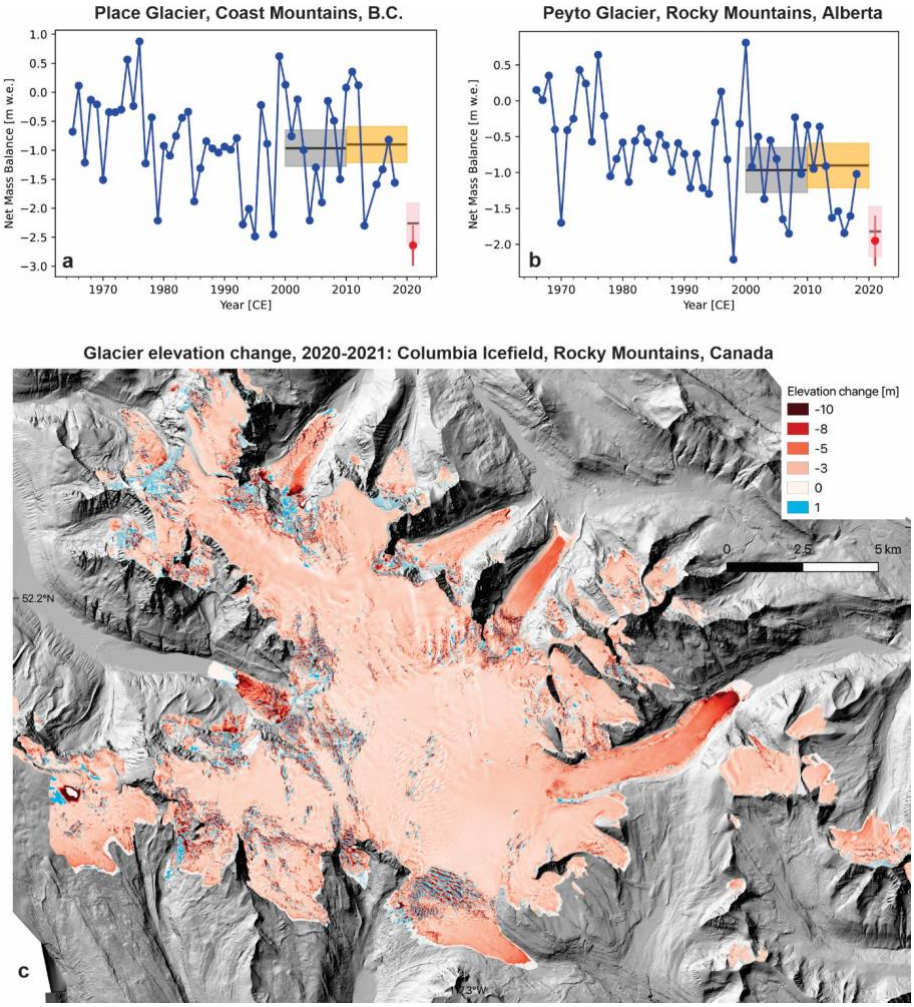

Figure 14: Glacier mass balance records from (a) Place Glacier, British Columbia, and (b) Peyto Glacier, Alberta from 1965 to 2021. Data for 1965-2019 are from the World Glacier Monitoring Service and 2021 mass balance estimates are from LiDAR surveys, with firn-density corrections after Pelto et al. (2019). The blue and yellow horizontal bars indicate decadal mean values for the region from Huggonet et al. (2021). Data from 2021 indicate the uncertainty (pink bar), the mass balance calculation using the contemporaneous LiDAR-derived glacier area (red circles), and the specific mass balance calculated from the Randolph Glacier Inventory glacier areas/outlines as used by Huggonet et al. (2021) (black crosshairs). (c) LiDAR-derived elevation change on the Columbia Icefield, Canadian Rocky Mountains, for the 2020-2021 mass balance year.

Reduced Glacier Melt Rates in the Swiss Alps:

Glaciers in the Swiss Alps suffered significantly less ice loss than in the previous years due to substantial snow in winter and a cool and rainy summer season. Nevertheless, in 2021 none of the monitored glaciers showed mass gain, and ice losses averaged around 0.5 m w.e., corresponding to a reduction of glacier ice volume in Switzerland of 0.8%.

Ice sheets

Ice sheets are expanses of glacial ice that cover an area larger than 50 000 km^2. In the current climate, there are two ice sheets, found on Greenland and Antarctica.

Greenland ice sheet

Changes in the total mass balance of the Greenland ice sheet reflect the combined effects of: surface mass balance, defined as the difference between snowfall and meltwater runoff from the ice sheet; the marine mass balance, which is the sum of mass losses at the periphery from the calving of icebergs and the melting of glacier tongues on contact with the ocean; and the basal mass balance,

which consists of basal melting due to geothermal heat, frictional heat generated by sliding at the base of the glacier and by deformation of the ice.

For Greenland[41], the total mass balance in 2020-2021 (1 September 2020 – 31 August 2021) was -166 Gt, which is close to the average for the period 1987-2021. This was the 25th year in a row with a negative mass balance. Over the period September 1986 to August 2021, for which we have daily data, the Greenland Ice Sheet lost a total of 5 511 Gt of ice. Cumulative mass loss was 4 261 Gt from April 2002 to June 2021, the period covered by observations from the GRACE satellites.

The GRACE and GRACE-FO satellites can measure changes in the amount of ice using the minute variations they cause in the gravitational field. This provides an independent measure of the total mass balance. Based on this data, the Greenland ice sheet for the same period as above (April 2002 to June 2021) has lost about 4 473 Gt. This ice loss contributed to a sea level rise of about 1.2 cm.

The surface mass balance for the 2020-2021 mass balance season in Greenland was +357 Gt, which is slightly above the 35-year average 1986-2020 of +326 Gt. However, estimated ice loss due to iceberg calving and glacier tongue melting, the marine mass balance, of -500 Gt, was the highest of the period. The basal mass balance is small (~ -23 Gt) and does not show an obvious trend. The Greenland surface mass balance record is now three and a half decades long and, although it varies considerably from one year to another, there has been an overall decline in the average surface mass balance and total mass balance over time.

Greenland Ice Sheet melt extent was close to the long-term average through the early summer, but temperatures and meltwater runoff were well above normal in late July and August 2021 (Figure 16), the latter event was associated with a major incursion of warm, humid air in mid-August. This air mass moved in from Baffin Bay and covered much of southwestern and central Greenland. On August 14, rain was observed for several hours at Summit Station, the highest point on the Greenland Ice Sheet (3 216 m), and air temperatures remained above freezing for about nine hours[42]. There is no previous report of rainfall at Summit, and this is the latest date in the year that above-freezing temperatures have been recorded at this location. Melt events at Summit were also observed in 1995, 2012, and 2019. Ice core records indicate that prior to 1995, the last time melting occurred at Summit was in the late 1800s.

[41] Based on the average of three regional climate and mass balance models. See Mankoff, K. D., X. Fettweis, P.L. Langen, M. Stendel, K.K. Kjeldsen, N.B. Karlsson, B. Noël, M.R. van den Broeke, W. Colgan, S.B. Simonsen, J.E. Box, A. Solgaard, A.P. Ahlstrøm, S.B. Andersen and R.S. Fausto, 2021: Greenland ice sheet mass balance from 1840 through next week. Earth Syst. Sci. Data, https://doi.org/10.5194/essd-2021-131, accepted.

[42] NSIDC (2021), http://nsidc.org/greenland-today/2021/08/rain-at-the-summit-of-greenland/

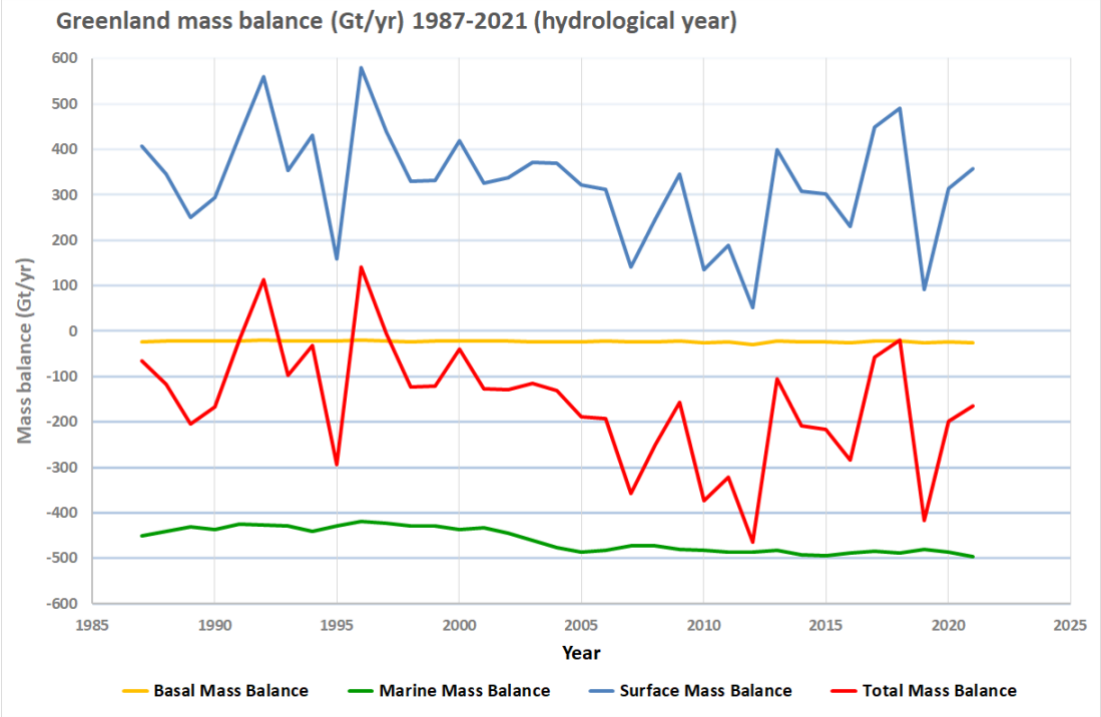

Figure 15: Components of the total mass balance of the Greenland Ice Sheet 1987-2021. Blue: Surface mass balance SMB, green: marine mass balance MMB (also referred to as discharge), orange: basal mass balance BMB, red: total mass balance TMB, the sum of SMB, MMB and BMB[43].

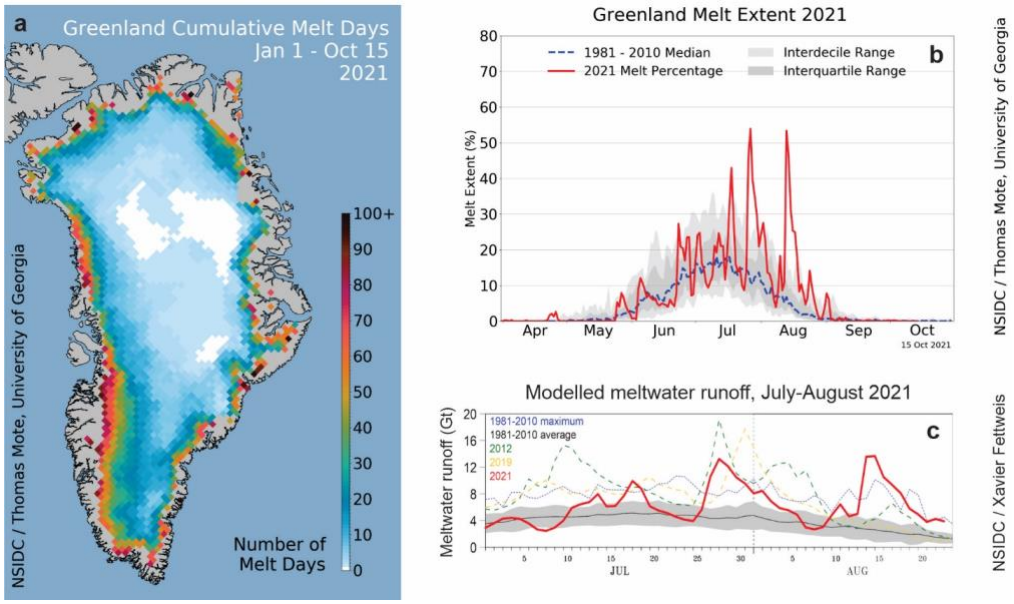

Figure 16: (a) Cumulative melt days on the Greenland Ice Sheet, 2021, indicating melt impacts over most of the ice sheet in summer 2021. (b) Melt extent (%) over the ice sheet through the 2021 melt season on Greenland, relative to the median melt extent from 1981-2010. (c) Greenland meltwater runoff through July-August 2021 relative to the recent extensive melt seasons of 2012 and 2019, indicating the record amount of late-season ice sheet melting associated with the mid-August rainfall event at Summit. All images are courtesy of the U.S. National Snow and Ice Data Center http://nsidc.org/greenland-today/, with thanks to Ted Scambos and the Greenland Ice Sheet Today. Analysis in (a) and (b) is from Thomas Mote, University of Georgia and meltwater runoff in (c) is estimated from the regional climate model MARv3.12, courtesy of Xavier Fettweis, University of Liège, Belgium.

[43] Mankoff, K D., X. Fettweis, P.L. Langen, M. Stendel, K.K. Kjeldsen, N.B. Karlsson, B. Noël, M.R. van den Broeke, W. Colgan, S.B. Simonsen, J.E. Box, A. Solgaard, A.P. Ahlstrøm, S.B. Andersen and R.S. Fausto, 2021: Greenland ice sheet mass balance from 1840 through next week, Earth Syst. Sci. Data, https://doi.org/10.5194/essd-2021-131, accepted.

Antarctic ice sheet

The Antarctic Ice Sheet so far experiences negligible surface melt compared to Greenland, but some melt typically occurs on the Antarctic Peninsula between November and February, as well as on some of the low-lying ice shelves and in coastal zones. The summer 2021 melt season in Antarctica was moderate and was below average for 1990-2020 (Figure 17)[44]. The northern Filchner Ice Shelf in the Weddell Sea experienced a strong but brief melt event in mid-December 2020. The summer melt season in Antarctica concluded in mid-February 2021. The strongest positive melt anomalies of the year were over the remnant Larsen B and C ice shelves on the Antarctic Peninsula; most other locations experienced near-normal melt extent relative to the mean 1990-2020 conditions.

Despite near-normal surface melting in Antarctica in summer 2021, GRACE-FO satellite gravity data indicate that the Antarctic Ice Sheet continued to lose mass in early 2021 (Figure 18), associated with calving and marine ice sheet melting in the Amundsen Sea sector of West Antarctica. Antarctic Ice Sheet mass loss since 2010 is largely driven by thinning and grounding-line retreat of Thwaites Glacier, triggered by ocean warming in this sector of the ice sheet[45].

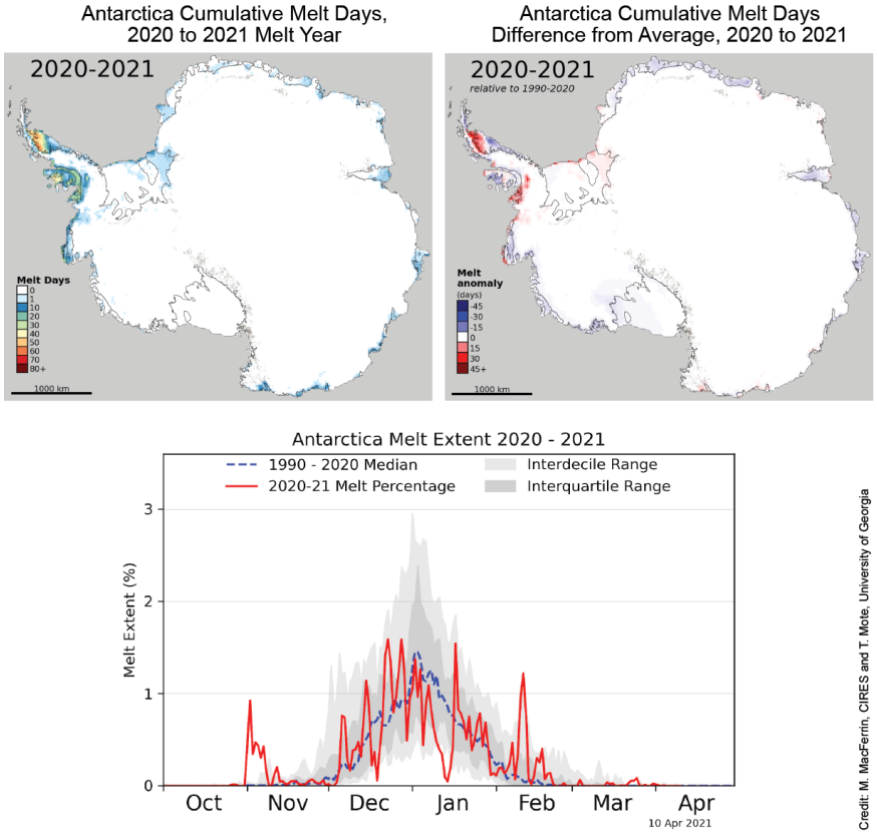

Figure 17: The 2021 melt season on the Antarctic Ice Sheet. Images courtesy of Michael MacFerrin and Thomas Mote, available from the NSIDC.

[44] http://nsidc.org/greenland-today/2021/04/the-antarctic-2020-to-2021-melt-season-in-review/

[45] Velicogna, I., Mohajerani, Y., A, G., Landerer, F., Mouginot, J., Noel, B., et al. (2020). Continuity of ice sheet mass loss in Greenland and Antarctica from the GRACE and GRACE Follow-On missions. Geophysical Research Letters, 47, e2020GL087291. https://doi.org/10.1029/2020GL087291, Rignot, E., J. Mouginot, Scheuchl, B., van den Broeke, M., van Wessem, M.J. and M. Morlighem (2019). Four decades of Antarctic Ice Sheet mass balance from 1979–2017. Proceedings of the National Academy of Sciences , 116 (4) 1095-1103; DOI: 10.1073/pnas.1812883116.

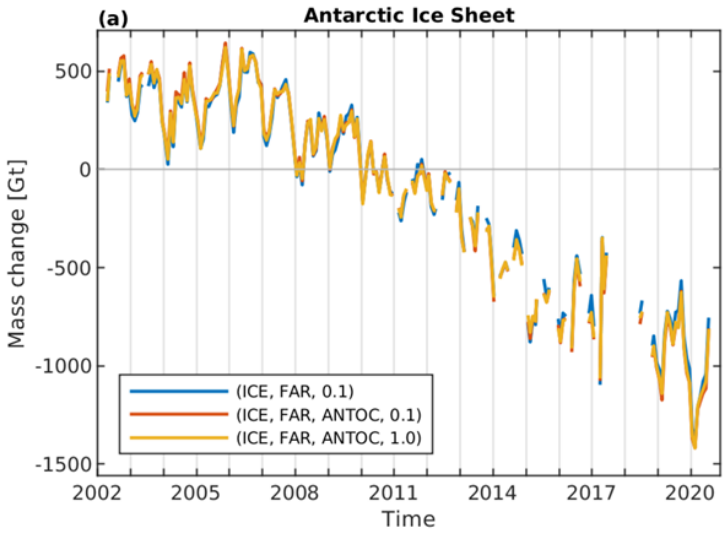

Figure 18: Antarctic Ice Sheet mass change measured by the GRACE and GRACE-FO satellite gravity missions, 2002-2021. The lines indicate different interpretations of the GRACE data (Groh and Horwath, 2021)[46].

Snow

Seasonal snow cover in the Northern Hemisphere has been experiencing a long-term decline in the late spring and summer, along with evidence of relative stability or increases in snow extent in the autumn (IPCC, 2021). Snow-cover extent (SCE) in 2021 was consistent with these long-term trends, with a May NH snow cover anomaly of -2 million km^2, the third lowest in the SCE record from 1970-2021 (Figure 19), based on analyses of the Rutgers Northern Hemisphere (NH) Snow Cover Extent (SCE) product[47]. The reduction in spring snow cover stands in contrast to the long-term trend and the most recent data for October. However, the IPCC AR6 note that the positive trends in Autumn snow cover in this data set were not replicated in other data sets[48].

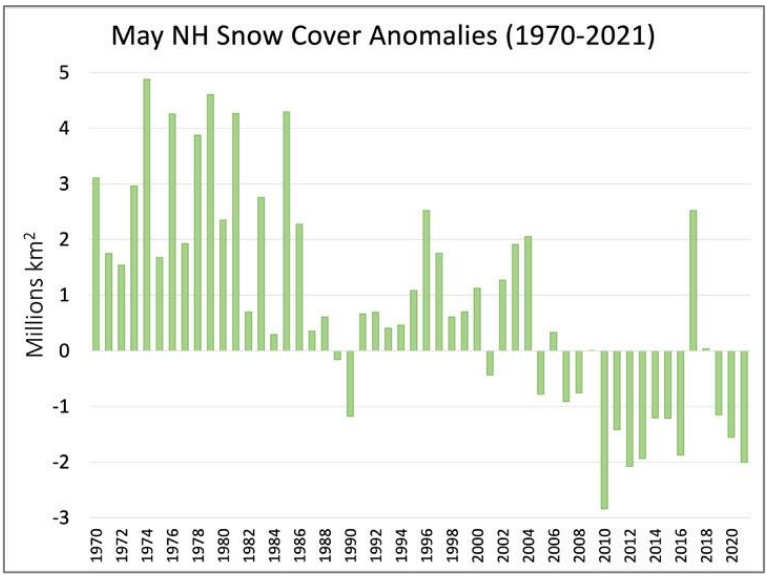

Figure 19: May snow-cover extent (SCE) anomaly in the Northern Hemisphere for the period 1970-2021, relative to the 1991-2020 average.

[46] Groh, A. and M. Horwath, 2021. Antarctic ice mass change products from GRACE/GRACE-FO using tailored sensitivity kernels. Remote Sensing 13 (9), 1736. https://doi.org/10.3390/rs13091736

[47] https://snowcover.org

[48] IPCC AR6 WG1 Chapter 9 pg 91 line 19-29.

Permafrost

Permafrost occurs beneath about one eighth of Earth's exposed land area. It is ground that remains at or below 0 °C for at least two consecutive years. Permafrost thaw can lead to landscape instability and other impacts, including the emission of greenhouse gases from previously frozen organic material. As permafrost temperature approaches 0 °C, changes in temperature in the ice-rich ground are subdued due to the phase change between ice and water. While temperature increase may level off near 0 °C for several years or decades due to the aforementioned phase change, the impacts of permafrost warming and thaw on ground stability including subsidence and mass movements, hydrology, ecosystems, and infrastructure are often clearly visible (Figure 20).

Figure 20: Recent slope instability associated with permafrost thaw, including active layer detachment slides and retrogressive thaw slumps. In the foreground, large amounts of material have pushed into the river to form a debris tongue. Foothills of the Mackenzie Mountains south of Norman Wells, north-western Canada. Image source: Government of Northwest Territories, Canada.

Since the 1990s, the Global Terrestrial Network for Permafrost (GTN-P) has compiled data sets of Permafrost Temperatures (temperature measured in boreholes) and Active Layer Thickness (the maximum thickness of the seasonally thawed layer above the permafrost). GTN-P products rely mostly on research projects to sustain activities. Long-term data series from national and regional networks operating in mountain and polar areas show a continuation of past warming trends up to 2020, the most recent data available.

Stratospheric ozone

Following the success of the Montreal Protocol, use of halons and CFCs has been reported as discontinued but their levels in the atmosphere continue to be monitored. Because of their long lifetime, these compounds will remain in the atmosphere for many decades and even if there were no new emissions, there is still more than enough chlorine and bromine present to cause complete destruction of ozone in Antarctica from August to December. As a result, the formation of the Antarctic ozone hole continues to be an annual spring event with year-to-year variation in its size and depth governed to a large degree by meteorological conditions.

The 2021 ozone hole developed relatively early and continued growing, resulting in a large and deep ozone hole. It expanded to 24 million km^2 on 24 September and remains close to this value as of mid-October 2021. The development of the hole, its extent and severity are close to that for the 2020 and 2018 seasons. The ozone hole reached its maximum area of 24.8 million km^2 on 7 October 2021 similar to the areas in 2020 and 2018 and close to the highest values observed in earlier years such as 28.2 million km^2 in 2015 and 29.6 million km^2 in 2006 according to an analysis from the National Aeronautics and Space Administration (NASA) (Figure 21a). NASA reported a minimum

ozone of 92 DU (Dobson Units) on 7 October 2021 which is the lowest value in the past 17 years (see Figure 21b). Since the end of September 2021, the concentration of stratospheric ozone was persistently reduced to near-zero values between 15 and 20 km altitude over Antarctica. Together with the season of 2020 these are some of the lowest ever ozone values measured via sondes at the Antarctic stations as reported by the National Oceanic and Atmospheric Administration (NOAA). The lowest total column value of 92 DU was reached on 7 October 2021. The unusually deep and large ozone hole this year is driven by a strong and stable polar vortex and very low temperatures in the stratosphere.

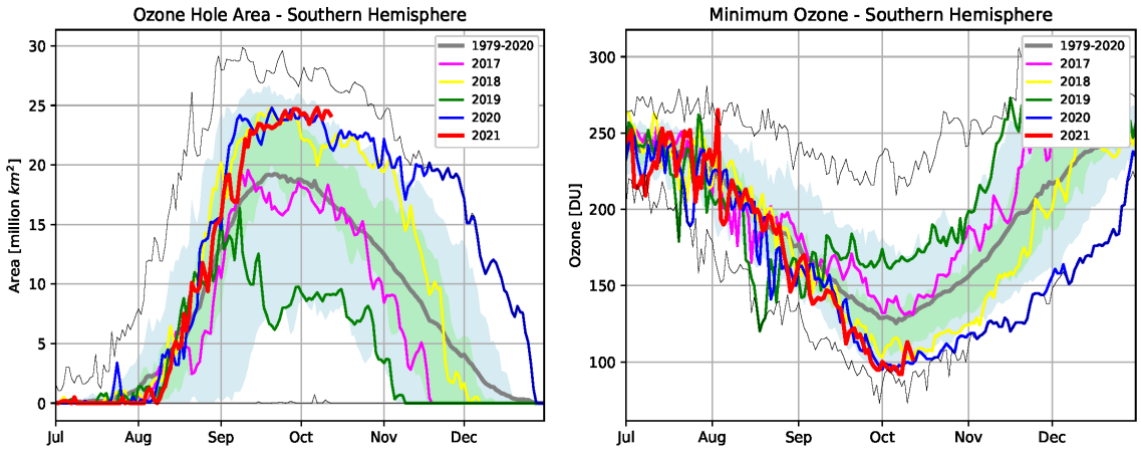

Figure 21: Area (millions of km²) and Minimum Ozone where the total ozone column is less than 220 Dobson units; 2021 is shown in red. The most recent years are shown for comparison as indicated by the legend. The smooth, thick grey line is the 1979–2020 average. The blue shaded area represents the 10th to 90th percentiles, and the green shaded area represents the 30th and 70th percentiles for the period 1979–2020. The thin black lines show the maximum and minimum values for each day in the 1979–2020 period. The plot is made at WMO on the basis of data downloaded from the NASA Ozone Watch (https://ozonewatch.gsfc.nasa.gov/). The NASA data are based on satellite observations from the OMI and TOMS instruments.

Drivers of short-term variability

There are many different natural phenomena, often referred to as climate patterns or climate modes, that affect weather at timescales ranging from days to several months. Surface temperatures change relatively slowly over the ocean, so recurring patterns in sea surface temperature can be used to understand and, in some cases, predict the more rapidly changing patterns of weather over land on seasonal time scales. Similarly, albeit at a faster rate, known pressure changes in the atmosphere can help explain certain regional weather patterns.

In 2021, the El Niño–Southern Oscillation (ENSO) and the Arctic Oscillation (AO) each contributed to major weather and climate events in different parts of the world and are described in further detail below.

ENSO El Niño Southern Oscillation

ENSO is one of the most important drivers of year-to-year variability in weather patterns worldwide. It is linked to hazards such as heavy rains, floods, and drought. El Niño, characterised by higher-than-average sea surface temperatures in the eastern tropical Pacific and a weakening of the trade winds, typically has a warming influence on global temperatures. La Niña, which is characterised by below-average sea surface temperatures in the central and eastern tropical Pacific and a strengthening of the trade winds, has the opposite effect.

La Niña conditions emerged in mid-2020 and peaked in the October–December period at moderate strength, with average sea surface temperatures 1.3 °C below the 1991–2020 normal. The La Niña

weakened through the first half of 2021, reaching an ENSO-neutral state (temperatures within 0.5 °C of normal) in May, according to both oceanic and atmospheric indicators. However, sea surface temperatures cooled after mid-year, approaching La Niña thresholds once again by October.

In addition to having a temporary cooling influence on Earth's global temperature, La Niña is associated with drier-than-normal conditions in east Africa; most of Kenya, Ethiopia, and Somalia experienced consecutive below-average rainfall seasons in late 2020 and early 2021, leading to drought in the region. In early 2021, precipitation was higher than normal over the Maritime Continent[49] and lower than normal in Patagonia at the beginning of the year, typical patterns associated with La Niña. Additionally, La Niña conditions can contribute to above-average hurricane activity in the North Atlantic, which has experienced 20 named tropical cyclones during its 2021 hurricane season to date (the 1981–2010 average for the entire season is 14), following a record-breaking season in 2020 (28 storms, also associated with La Niña).

AO Arctic Oscillation

The AO is a large-scale atmospheric pattern that influences weather throughout the Northern Hemisphere. The positive phase is characterised by lower-than-average air pressure over the Arctic and higher-than-average pressure over the northern Pacific and Atlantic Oceans. The jet stream is parallel to the lines of latitude and farther north than average, locking up cold Arctic air, and storms can be shifted northward of their usual paths. The mid-latitudes of North America, Europe, Siberia, and East Asia generally see fewer cold air outbreaks than usual during the positive phase of the AO. A negative AO has the opposite effect, associated with a more meandering jet stream and cold air spilling south into the mid-latitudes where the jet stream dips southward.

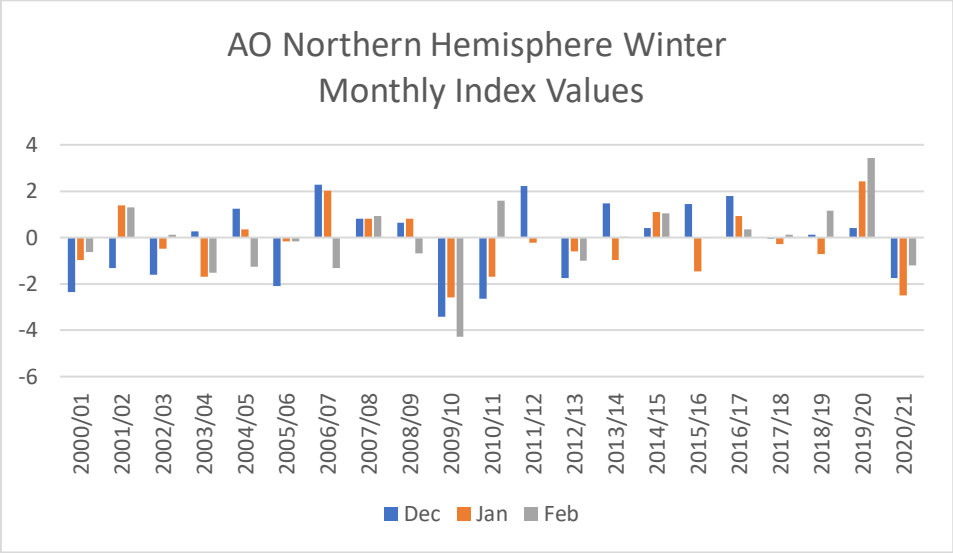

Figure 22: Arctic Oscillation monthly index values for Northern Hemisphere winter months, December in blue, January in orange and February in grey (Source: NOAA Climate Prediction Center).

The AO was negative during the Northern Hemisphere 2020-21 winter and, seasonally, was the most negative on record since winter 2009-10. The jet stream swept down over North America, contributing to its coldest February for the continent since 1994. However, the same wavy jet stream also contributed to extreme warmth in parts of northern and eastern Asia in February as it surged northward over the area, with regions in Mongolia, China, Japan, and the Republic of Korea reporting record-high temperatures for this time of year. The contrast between the positive AO

[49] The Maritime Continent refers to the islands found between mainland southeast Asia and Australia in the eastern Indian Ocean and western Pacific. It covers a similar area to the Malay Archipelago.

(winter 2019-20) and the negative AO (winter 2020-21) could explain some of the differences between temperature patterns in the first quarters of 2020 and 2021. The negative winter phase of the Arctic Oscillation has also been linked to more moderate Arctic sea ice loss the following summer[50] (see Arctic sea ice). The minimum extent for 2021, reached on 16 September, was the 12th lowest extent on record and the highest minimum since 2014.

High impact events in 2021

Although understanding broad-scale changes in the climate is important, the most acute impacts of weather and climate are often felt during extreme meteorological events such as heavy rain and snow, droughts, heatwaves, cold waves, and storms, including tropical storms and cyclones. These can lead to or exacerbate other high-impact events such as flooding, landslides, wildfires, and avalanches. This section is based largely on inputs from WMO Members. The risks and impacts associated with these events are described in Risks and impacts.

Heatwaves and wildfires

Exceptional heatwaves affected western North America on several occasions during June and July. By some measures, the most extreme was in late June in the north-western United States and western Canada. Lytton, in south-central British Columbia, reached 49.6 °C on 29 June, breaking the previous Canadian national record by 4.6 °C, with temperatures reaching the mid-40s as far west as eastern suburbs of Vancouver and in the interior of Vancouver Island. It was also more than 5 °C higher than the previous highest known temperature north of 50 °N. 569 heat-related deaths were reported in British Columbia alone between 20 June and 29 July[51]. Many long-term stations broke records by 4 to 6 °C, including Portland, Oregon (46.7 °C). There were also multiple heatwaves in the southwestern United States. Death Valley, California reached 54.4 °C on 9 July, equalling a similar 2020 value as the highest recorded in the world since at least the 1930s. It went on to be the hottest summer on record averaged over the continental United States.

There were numerous major wildfires during and after the heatwaves (including one which largely destroyed the town of Lytton the day after its record temperature). The Dixie fire in northern California, which started on 13 July, had burned about 390,000 hectares by 7 October, the largest single fire on record in California. However, the overall area burned for the season[52] in the United States was slightly below average[53].

Extreme heat affected the broader Mediterranean region on several occasions during the second half of the Northern Hemisphere summer. The most exceptional heat was in the second week of August. On 11 August, an agrometeorological station near Syracuse in Sicily reached 48.8 °C, a provisional European record, while Kairouan (Tunisia) reached a record 50.3 °C. Montoro (47.4 °C) set a national record for Spain on 14 August, while on the same day Madrid (Barajas Airport) had its hottest day on record with 42.7 °C. Earlier, on 20 July, Cizre (49.1 °C) set a Turkish national record and Tbilisi (Georgia) had its hottest day on record (40.6 °C). Major wildfires occurred across many parts of the region with Algeria, southern Turkey and Greece especially badly affected. Over 40

[50] Rigor, I. G., Wallace, J. M., & Colony, R. L. (2002). Response of sea ice to the Arctic Oscillation. Journal of Climate, 15(18), 2648–2663. https://doi.org/10.1175/1520-0442(2002)015<2648:ROSITT>2.0.CO;2

[51] https://www2.gov.bc.ca/gov/content/life-events/death/coroners-service/news-and-updates/heat-related

[52] As of 8 October.

[53] National Interagency Fire Center

deaths occurred in the Algerian fires. Other countries which experienced significant wildfires during the period included France, Italy, North Macedonia, Lebanon, Israel, Libya, Tunisia and Morocco.

June was exceptionally warm through many parts of eastern Europe. National June records were set for Estonia (34.6 °C) and Belarus (37.1 °C), whilst locations which had their hottest June day on record included St. Petersburg (35.9 °C) and Moscow (34.8 °C), both on 23 June, Yerevan (Armenia, 41.1 °C) on the 24th, and Baku (Azerbaijan, 40.5 °C) on the 26th. Tampere in Finland reported its highest temperature on record (33.2 °C) on 22 June. Libya also saw a prolonged heatwave in late June. Later in the summer, abnormal warmth also reached northwest Europe; 31.3 °C at Castlederg on 21 July was a record for Northern Ireland.

For the third successive year, there were major wildfires during the summer in Siberia, particularly in the Sakha Republic around Yakutsk. Fire activity in the Amazon region during the August-September peak season was less than in 2019 or 2020[54], but there was extensive fire activity in other parts of Brazil including the Pantanal. The Australian wildfire season in 2020-21 was also relatively inactive after a very severe season in 2019-20.

Cold spells and snow

Abnormally cold conditions affected many parts of the central United States and northern Mexico in mid-February. The most severe impacts were in Texas, which generally experienced its lowest temperatures since at least 1989, with temperatures in some areas staying below freezing continuously for 6 to 9 days, setting records in locations including Austin and Waco. On 16 February, Oklahoma City reached −25.6 °C and Dallas −18.9 °C, their lowest temperatures since 1899 and 1949 respectively. Electricity transmission was severely disrupted, with power outages affecting nearly 10 million people at the event's peak, while frozen pipes were another major cause of damage. 172 deaths were reported in the United States along with over $20 billion in economic losses, making it the most costly winter storm on record for the United States[55].

It was a cold winter in many parts of northern Asia. The Russian Federation had its coldest winter since 2009-10. Below-average temperatures affected much of Japan in late December and early January, with heavy snowfalls on a number of occasions, and a number of locations on the Sea of Japan coast of Honshu having their heaviest 72-hour snowfall on record in early January. Much of China was also cold during this period, with Beijing reaching −19.6 °C on 7 January, its lowest temperature since 1966.

A severe snowstorm hit many parts of Spain from 7 to 10 January, followed by a week of freezing air temperatures. A total of 53 cm of snow fell at the central city location of Retiro, and heavy falls were also reported in many other parts of Spain[56]. Some locations, including Toledo (−13.4 °C) and Teruel (−21.0 °C), had their lowest temperatures on record on 12 January in the wake of the storm. There were major disruptions to land and air transport. Later in the winter, in the second week of February, the Netherlands experienced its most significant snowstorm since 2010 with heavy snow also falling in Germany, Poland and the United Kingdom; in the wake of the storm, Braemar recorded −23.0 °C on 12 February, the lowest temperature in the United Kingdom since 1995. In southeast Europe, Athens had its heaviest snow since 2009 on 15 February.

An abnormal spring cold outbreak affected many parts of Europe in early April. Record low April temperatures in France included −7.4 °C at Saint-Etienne on the 8th and −6.9 °C at Beauvais on the

[54] https://queimadas.dgi.inpe.br/queimadas/portal-static/estatisticas_estados/
[55] https://www.ncdc.noaa.gov/billions/events/US/2021
[56] http://www.aemet.es/en/conocermas/borrascas/2020-2021/estudios_e_impactos/filomena

6th, while Belgrade (Serbia) had its heaviest April snowfall on record on the 7th. At high elevations, national records for April were set for Switzerland (−26.3 °C at Jungfraujoch) and Slovenia (−20.6 °C at Nova vas na Blokah). This followed a very warm end to March with France having its warmest March day on record on the 31st. Frost damage to agriculture was widespread and severe, with losses to vineyards and other crops in France alone exceeding US$4.6 billion[57]. The United Kingdom went on to have its lowest monthly mean temperature for April since 1922.

Precipitation

Compared to temperature, precipitation is characterized by higher spatial and temporal variability. Large regions with above normal (1951-2000) precipitation totals from January till September were Eastern Europe, Southeast Asia, the Maritime Continent, areas of northern South America and south-eastern North America (Figure 24). Large regions with a rainfall deficit included southwest Asia and the Middle East, parts of southern Africa, southern South America and central North America.

La Niña events are often – but not always – characterised by shifting patterns of rainfall. In some regions the pattern of precipitation anomalies were typical of those associated with La Niña conditions at the beginning of the year: wetter than average conditions over the Maritime Continent and drier than usual conditions in Patagonia. However, in Australia, where La Niña is typically associated with above-normal rainfall, precipitation anomalies were relatively weak.

The onset of the African Monsoon was delayed. Later in the season, rainfall totals were higher than normal, especially in the western monsoon region. In total, the seasonal rainfall was close to normal.

In Southern Africa, in an area centred on Zambia, rainfall amounts during the wet season until May were below the long-term mean. It was at least the second year in a row with below normal rainfall for Madagascar; rainfall totals have been below average in most years since 2011. In addition, the April-May wet season was drier than usual in the Greater Horn of Africa region.

Over North America, above average rainfall totals were observed in Alaska and the north of Canada, and in the southeast of the United States and parts of the Caribbean. Between these two wetter-than-average bands was a swath of unusually dry conditions extending across the width of the continent.

Unusually high precipitation amounts, relative to the chosen climatology period (1951-2010), were recorded in the southwest and southeast of Australia. On the other hand, abnormally low precipitation amounts were received on the North Island of New Zealand.

Unusually low precipitation amounts fell around the Mediterranean Sea, while unusually high totals were detected around the Black Sea and in parts of Eastern Europe.

[57] French national contribution

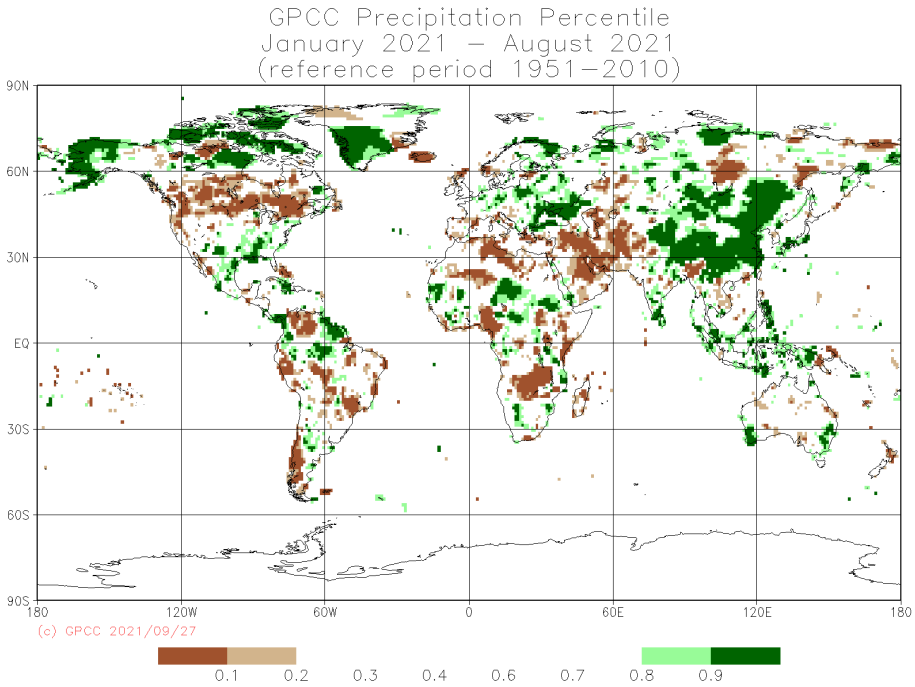

Figure 23: Total precipitation in Jan-Aug 2021, expressed as a percentile of the 1951–2010 reference period, for areas that would have been in the driest 20% (brown) and wettest 20% (green) of years during the reference period, with darker shades of brown and green indicating the driest and wettest 10%, respectively (Source: Global Precipitation Climatology Centre (GPCC), Deutscher Wetterdienst, Germany)

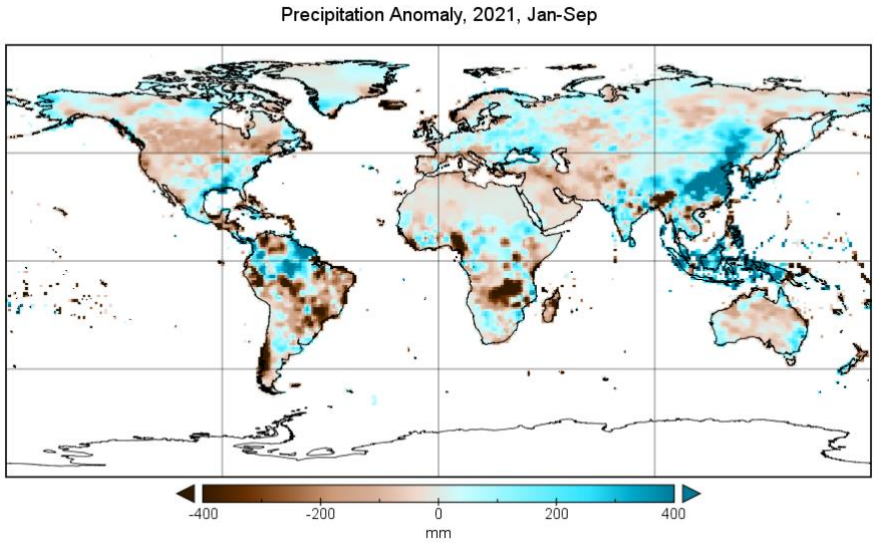

Figure 24: Total precipitation anomaly in Jan-Sep 2021 w.r.t. reference period 1951-2000. Blue indicates more precipitation than the long-term means while brown indicates less than usual rainfall totals. The darkness of the colour represents the amount of the deviation. (Source: Global Precipitation Climatology Centre (GPCC), Deutscher Wetterdienst, Germany).

Flood

Extreme rainfall, to which moisture ahead of Typhoon In-fa contributed, hit Henan Province of China from 17 to 21 July. The most severely affected area was around the city of Zhengzhou, which on 20 July received 201.9 mm of rainfall in one hour (a Chinese national record), 382 mm in 6 hours, and 720 mm for the event as a whole, more than its annual average. The city experienced extreme flash

flooding with many buildings, roads and subways inundated. 302 deaths were attributed to the flooding, and economic losses of US$17.7 billion were reported[58].

Western Europe experienced some of its most severe flooding on record in mid-July. The worst-affected area was western Germany and eastern Belgium, where 100 to 150 mm fell over a wide area on 14-15 July over ground which was already unusually wet after high recent rainfall. The highest daily rainfall was 162.4 mm at Wipperfürth-Gardenau (Germany). Numerous rivers experienced extreme flooding, with several towns inundated, and there were also several landslides. France, the Netherlands, Luxembourg, the United Kingdom and Switzerland also experienced significant flooding. 179 deaths were reported in Germany and 36 in Belgium, with economic losses in Germany exceeding US$20 billion[59].

Persistent heavy rainfall in mid-March resulted in major flooding in eastern New South Wales in Australia[60]. The week from 18 to 24 March was the wettest on record averaged over coastal New South Wales. The most severe flooding was in the Hastings, Karuah and Manning Rivers north of Sydney, but there was also significant flooding in other areas, including parts of western Sydney. There was also flooding on many inland rivers, which led to substantial recovery in water storages severely depleted by the 2017-19 drought. At least US$2.1 billion in economic losses were reported.

Two flash flood events associated with localised heavy rainfall occurred in Afghanistan during 2021, in early May around Herat in the west, and on 28-29 July centred on Nuristan in the east. There was significant loss of life in both events with 61 deaths reported in the May event and 113 in the July event[61].

Flash flooding occurred on several occasions around the Mediterranean and Black Sea coasts. The most impactful event was on the Black Sea coast of Turkey on 10 August, where several towns experienced severe damage and 77 deaths were reported. 399.9 mm of rain fell at Bozkurt in 24 hours. This event was associated with a 'Medicane' – a storm forming outside the tropics that nevertheless has characteristics of a tropical storm – in the Black Sea, with heavy rain and flooding also reported on the Russian Black Sea coast. On 4 October, exceptional rainfall fell in coastal regions of Liguria (northwest Italy), including 496.0 mm in 6 hours at Montenotte Inferiore and 740.6 mm in 12 hours at Rossiglione.

Persistent above-average rainfall in the first half of the year in parts of northern South America, particularly the northern Amazon basin, led to significant and long-lived flooding in the region. The Rio Negro at Manaus (Brazil) reached its highest level on record, peaking at 30.02 m on 20 June[62]. The most widespread flooding was reported in northern Brazil, but Guyana, Colombia and Venezuela were also affected.

The progress and withdrawal of the Indian Monsoon was delayed but overall Indian monsoon rainfall was close to average, with above-average falls in the west offset by below-average values in the northeast. During the course of the season, 529 deaths in India and 198 in Pakistan (as of 30 September) were attributed to flooding with further deaths in Bangladesh and Nepal[63]. In eastern Asia, eastern China (except for Henan) was generally less wet during the monsoon season than in

[58] RM 114.3 billion, from the Chinese national contribution
[59] German national contribution
[60] http://www.bom.gov.au/climate/current/statements/scs74.pdf?20210621
[61] EM-DAT
[62] http://www.cprm.gov.br/sace/boletins/Amazonas/20211022_11-20211025%20-%20114229.pdf
[63] National contributions for India and Pakistan, EM-DAT has 120 deaths in Nepal over two incidents and 21 in Bangladesh from one,

2020, but August was extremely wet in Japan. Western Japan had its wettest August on record[64], with some locations having more than 1400 mm of rain between 11 and 26 August.

The rainy season in the African Sahel was generally close to the average (1951-2000), and less wet than some recent years, although there was still some significant flooding reported, especially in Niger, Sudan and South Sudan as well as Mali. Elsewhere in Africa, Lake Tanganyika rose to more than 3 m above its normal level in May[65], displacing lakeshore residents in Burundi. In southern Africa, much of which had been experiencing long-term drought, rainfall during the 2020-21 rainy season was above average in regions including northern South Africa and Zimbabwe with some flooding reported but was near or below average further north.

Drought

Significant drought affected much of subtropical South America for the second successive year. Rainfall was well below average over much of central and southern Brazil[66], Paraguay, Uruguay and northern Argentina. The drought led to significant agricultural losses, exacerbated by a cold outbreak at the end of July, in which maximum temperatures were below 10°C for five consecutive days over higher parts of the south and which caused damage over many of Brazil's coffee-growing regions. Low river levels also reduced hydroelectricity production[67] and disrupted river transport. The Brazilian government declared a situation of critical scarcity of water resources in the Paraná hydrographic region, with numerous water storages at or near their lowest levels in the last 20 years[68]. The 24-month Standardised Precipitation Index (SPI) over the region reached its lowest level since the 1960s. The Paraguay River at Asuncion fell to a record low 0.75 m below the reference level on 6 October, 0.21 m below the previous record set last year. In Chile, where long-term drought has persisted for most of the last decade, 2021 was another dry year, with most locations having rainfall at least 30% below average. At Santiago, 107.7 mm had fallen as of 6 October, 67% below average.

Widespread drought in western North America, which had become established during 2020, spread and intensified in 2021. By September, extreme to exceptional drought covered most of the United States over and west of the Rocky Mountains, despite some slight easing from July onwards in parts of the inland southwest, due to an active summer monsoon. Extreme to exceptional drought also extended eastwards on both sides of the United States-Canada border, affecting northern border states as far east as Minnesota and the Prairie Provinces of Canada. The 20 months from January 2020 to August 2021 was the driest on record for the southwestern United States[69], more than 10% below the previous record. Forecast wheat and canola crop production for Canada in 2021 is 30 to 40% below 2020 levels[70], whilst in the United States, the level of Lake Mead on the Colorado River fell in July to 47 m below full supply level, the lowest level on record since the reservoir was fully commissioned.

Significant drought affected large areas of southwest Asia during 2021. Well below average precipitation fell during the 2020-21 cool season in regions including most of Iran, Afghanistan, Pakistan, southeast Turkey, and Turkmenistan. Pakistan had its third-driest February on record. Mountain snowpack was also well below average, with snow cover extent in Iran about half the

[64] https://ds.data.jma.go.jp/tcc/tcc/news/press_20210924.pdf
[65] Reliefweb: https://reliefweb.int/disaster/fl-2021-000039-bdi
[66] https://clima.inmet.gov.br/prec
[67] http://www.ons.org.br/Paginas/Noticias/20210707-escassez-hidrica-2021.aspx
[68] https://www.gov.br/ana/pt-br/assuntos/noticias-e-eventos/noticias/ana-declara-situacao-de-escassez-quantitativa-dos-recursos-hidricos-da-regiao-hidrografica-do-parana
[69] https://www.drought.gov/news/new-noaa-report-exceptional-southwest-drought-exacerbated-human-caused-warming
[70] https://www150.statcan.gc.ca/n1/daily-quotidien/210914/dq210914b-eng.htm

long-term average for most of January and February, leading to reduced streamflow in rivers depending on snowmelt, and reduced water availability for irrigation.

A severe, relatively localised, drought, which has persisted for at least two years, continues to affect southern Madagascar[71]. Rainfall for the 12 months from July 2020 to June 2021 was around 50% below normal over the region. There were significant food security issues in the area, with 1.14 million classified by the World Food Programme as needing urgent assistance as of August 2021[72].

Tropical cyclones

Tropical cyclone activity over the globe in 2021 was close to average (1981-2010). For the second successive year, the North Atlantic had a very active season, with 20 named storms as of 11 October, about double the average for that period. It was also an active season in the North Indian Ocean, but the western North Pacific and eastern North Pacific were near to or below average. The 2020-21 Southern Hemisphere season was also slightly below average in both the Pacific and Indian Oceans.

The most significant hurricane of the North Atlantic season was Ida. Ida made landfall as a category 4 system in Louisiana on 29 August with sustained 1-minute winds of 240 km/h, the equal-strongest landfall on record for the state, with major wind damage and storm surge inundation. The system then continued on a northeast track over land with significant flooding, especially in the New York City area. New York, which had already experienced flooding from Hurricane Henri two weeks earlier, had a record hourly rainfall of 80 mm, with 24-hour totals exceeding 200 mm in parts of the city. Before it developed into a tropical cyclone, Ida's precursor system also caused significant flooding in Venezuela. In total, 72 direct and 43 indirect deaths were attributed to Ida in the United States and Venezuela, with economic losses in the United States estimated at US$63.8 billion[73]. Another significant landfall during the season was Grace, which hit Veracruz (Mexico) as a category 3 hurricane, having earlier resulted in impacts, mostly from flooding, in Haiti (where it hindered post-earthquake recovery), the Dominican Republic, Jamaica, and Trinidad and Tobago.

In the Southern Hemisphere, 2021's most significant cyclone[74] was Seroja in April. Seroja formed south of Indonesia and tracked southeast towards Western Australia. It made landfall near Kalbarri on 11 April as an (Australian) category 3 cyclone, the strongest landfall so far south in Western Australia since 1956. Seroja's most severe impacts were from flooding and associated landslides from its precursor system in Timor-Leste, and the Indonesian regions of East Nusa Tenggara, Flores and Timor. Kupang (Timor) received 700.4 mm rainfall in the four days from 2 to 5 April. 272 deaths in total were attributed to Seroja, 230 in Indonesia, 41 in Timor-Leste and one in Australia[75]. Eloise in January contributed to flooding in southern Africa with damage and casualties reported in Mozambique, South Africa, Zimbabwe, Eswatini and Madagascar, while in the South Pacific, Ana and Niran caused flooding and power outages in Fiji and New Caledonia respectively.

The most severe cyclone of the North Indian Ocean season was Tauktae, which tracked north off the west coast of India, with a peak 3-minute sustained wind speed[76] of 50-53 m/s, before making landfall in Gujarat on 17 May at slightly below peak intensity, the equal strongest known landfall in Gujarat. At least 144 deaths were reported in India and 4 in Pakistan[77]. Later in the season, Cyclone Gulab crossed the eastern coast of India from the Bay of Bengal in late September; the remnant

[71] https://reliefweb.int/sites/reliefweb.int/files/resources/cb7310en.pdf
[72] https://reliefweb.int/sites/reliefweb.int/files/resources/WFP%20Madagascar%20Country%20Brief%20-%20August%202021.pdf
[73] https://www.ncdc.noaa.gov/billions/events/US/2021
[74] Tropical Cyclone Yasa (December 2020) forms part of 2020-21 seasonal statistics but was reported on in the 2020 State of the Climate.
[75] EM-DAT
[76] https://rsmcnewdelhi.imd.gov.in/uploads/report/26/26_e0cc1a_Preliminary%20Report%20on%20ESCS%20TAUKTAE-19july.pdf
[77] From national contributions

system crossed India before emerging and re-intensifying in the Arabian Sea, where it was renamed Shaheen. Shaheen made landfall on 3 October on the northern Oman coast northwest of Muscat, the first cyclone since 1890 to make landfall in this area. Al Suwaiq recorded 294 mm rain in 24 hours, about three times the region's annual average. 39 deaths were reported across India, Pakistan, Oman and Iran, mostly from flooding.

Direct impacts from North Pacific tropical cyclones were less than in recent years, although there were several significant landfalls, most notably from Typhoon Chanthu on the Batanes Islands (Philippines). Chanthu and Typhoon In-fa, in July, also both contributed to flooding and disruptions to shipping around Shanghai, while moisture ahead of In-fa was a contributor to the Henan Province floods (see Flood), and Dianmu contributed to flooding in Thailand in September after making landfall in Viet Nam.

Severe storms

There were multiple severe thunderstorm outbreaks in western and central Europe in the second half of June. An F4 tornado[78] struck several villages in southern Moravia on 24 June, with major damage and six deaths reported. This was the strongest tornado on record in the Czech Republic. Tornadoes were also reported during the month in Belgium and France. Large hail (6-8 cm in diameter) was reported in multiple countries, including the Czech Republic, Slovakia, Switzerland, and Germany. In the Czech Republic alone, losses were around US$ 700 million.

959 tornadoes were provisionally reported in the United States between January and April, slightly below the 1991-2010 average. The most significant outbreak, including the season's only EF-4 tornado[78], hit the southeast on 25 March with the most severe impacts in Alabama and western Georgia. 6 deaths and US$1.6 billion in economic losses were reported. Hailstorms in Texas and Oklahoma on 27-28 April resulted in US$2.4 billion in losses.

Attribution

Attribution of individual extreme events can often take several months to complete peer review. But increasingly it is becoming possible to carry out rapid attribution assessments that used peer-reviewed methods to reach conclusions within just a few days of a weather record being broken. Such "rapid attribution" studies have been carried out for the heatwave in northwest America in June and July[79,80] and of floods in western Europe in July[81]. Studies of the heatwave in the Pacific Northwest found that while the heatwave is still quite rare in today's climate, it would have been virtually impossible without climate change.

For the western Europe flooding, the rapid attribution study found that the detection of trends in extreme precipitation at the scale of the event in question was challenging and that saturated soils and the local hydrology were also factors in the event. However, across a wider area of western Europe, significant trends in extreme precipitation were found and these could be attributed to human-induced climate change and the study concluded that human-induced climate change had increased the likelihood of such an event.

---

[78] On both the Fujita scale and the Enhanced Fujita scale, a tornado that causes devastating damage is classified as category 4 tornado (F4 and EF4 respectively). The scales differ in the wind speeds thought to be associated with "devastating damage" with lower wind speeds assumed in the Enhanced system for the same level of damage.

[79] https://www.worldweatherattribution.org/western-north-american-extreme-heat-virtually-impossible-without-human-caused-climate-change/

[80] https://blog.metoffice.gov.uk/2021/06/29/heatwave-record-for-pacific-north-west/

[81] https://www.worldweatherattribution.org/heavy-rainfall-which-led-to-severe-flooding-in-western-europe-made-more-likely-by-climate-change/

More generally, events such as these fit into a broader pattern of change. The IPCC assessed[82] that hot extremes in the regions of West North America and Northwest North American have increased, and that there is at least medium confidence in a human contribution to this increase. Similarly, the IPCC assessed that heavy precipitation has increased in the West and Central Europe region affected by flooding, but that there is currently low confidence in the attribution of this change to human influence.

Risks and impacts

The risk of climate-related impacts depends on complex interactions between climate-related hazards and the vulnerability, exposure and adaptive capacity of human and natural systems. At current levels of global greenhouse gas emissions, the world remains on course to exceed the agreed temperature thresholds of either 1.5 °C or 2 °C above pre-industrial levels, which would increase the risks of pervasive climate change impacts beyond what is already seen.

State of disasters

Disasters continue to take a heavy toll on life and assets, severely affecting and rolling back the development gains of countries. Years of investment in disaster preparedness, including early warning and rapid response capabilities, has strengthened capacities to reduce the human impact of disasters. However, economic losses remain high and continue to increase. The impact of high-frequency, low-impact events has also increased, often cumulatively exceeding the impact of single mega events.

Human impact of disasters

In the longer term, the average annual number of dead and missing persons in the event of disaster per 100 000 people has fallen from 1.98 during 2005-2014 to 1.32 during 2011-2020. Nonetheless, in absolute terms the disaster-related mortality remains high. In the last three years alone (2018-2020), a total of about 250 000 disaster-related deaths and missing persons were reported by an average of 74 countries[83].

The single largest event with highest mortality in 2021 was the earthquake in Haiti resulting in over 2500 deaths. However, the impact of climate change and variability continues to manifest in the form of hydrometeorological disasters. In 2021, floods resulted in around 1200 deaths in India, over 350 deaths in China, and over 200 deaths in Germany and Belgium. At the same time, over 600 people lost their lives due to heat waves in Northern America[84].

In the last three years (2018-2020), a total of approximately 319 million people were affected due to disasters as reported by an average of 66 countries each year[83]. In 2020 alone, 40.5 million new internal displacements were recorded, of which over 75 per cent were displaced due to disaster[85].

Driven by climate, growing vulnerability and conflict, humanitarian needs are at their highest-ever with one in every 33 people globally in need of assistance and protection[86]. Recurrent droughts continue to affect millions of people around the world, in particular in countries in Africa and Asia[84].

[82] IPCC AR6 WG1 Summary for Policymakers Figure SPM.3

[83] SFM: Sendai Framework Monitor https://sendaimonitor.undrr.org/ and https://desinventar.net
[84] EMDAT: https://public.emdat.be
[85] https://www.internal-displacement.org/global-report/grid2021/
[86] https://gho.unocha.org/

Economic cost of disasters

In the last three years (2018-2020), total economic losses of about US$ 148.32 billion have been reported by an average of 53 countries each year[83]. That this is an underestimation (due to limited reporting on loss and damage), can be ascertained from the fact that global disaster losses from natural hazards in 2020 alone is estimated to be US$210 billion by the insurance sector, which was over 25% higher than in the previous year[87]. In fact, over a four-decade period starting 1980, total losses due to such disasters have been estimated to be US$5.2 trillion[88].

In 2019, the agriculture sector accounted for 60 per cent of recorded losses, followed by the housing infrastructure sector[83]. The Food and Agriculture Organization (FAO) estimates that between 2008 and 2018, disasters cost the agricultural sectors of developing-country economies over US$108 billion in damaged or lost crop and livestock production[89]. At a global level, disaster-related losses amounted to US$280 billion. Up to 4% of the agricultural production was lost to disasters and 82% of all damage caused by drought was absorbed by the agricultural sector.

89.93 million people were reported to have lost or had livelihoods affected by disasters during 2018-2020. These figures do not yet consider the COVID-19 impact which is expected to significantly push the poverty figures - an estimated additional 97 million people dropped below the poverty line in 2020[90]. This, in combination with extreme weather events, including drought – is having devastating effects on global hunger and poverty.

Further, in 2019, Least Developed Countries accounted for about 21% of reported mortality and 5% of economic losses which is relatively higher as compared to their total population and GDP.

Food Security

Global outlook of food security in 2021

In the last ten years, conflict, extreme weather events and economic shocks have increased in frequency and intensity. The compound effects of these perils, further exacerbated by the COVID-19 pandemic, have led to a rise in hunger and, consequently, undermined decades of progress towards improving food security (Figure 25). Worsening humanitarian crises in 2021 have also led to a growing number of countries at risk of famine. Following a peak in undernourishment in 2020 (768 million people), projections indicated a decline in global hunger to around 710 million in 2021 (9%)[91]. However, as of October 2021, the numbers in many countries were already higher than in 2020. This striking increase (19%) was mostly felt among groups already suffering from food crises or worse (IPC/CH Phase 3 or above), rising from 135 million people in 2020 to 161 million by September 2021[92]. Another dire consequence of these shocks was the growing number of people facing starvation and a total collapse of livelihoods (IPC/CH Phase 5), mostly in Ethiopia, South Sudan, Yemen, and Madagascar (584 000 people). The first quarter of 2021 has also seen the highest global consumer food prices in the last six years, concentrated in Latin America and the Caribbean[91]. In West Africa, prices of coarse grains increased, driving food prices to record and near record highs in several countries, exacerbated by civil insecurity and torrential rains. In North Africa, food inflation

[87] https://www.munichre.com/en/company/media-relations/media-information-and-corporate-news/media-information/2021/2020-natural-disasters-balance.html

[88] https://www.munichre.com/en/risks/natural-disasters-losses-are-trending-upwards.html

[89] FAO. 2021. The impact of disasters and crises on agriculture and food security: 2021. Rome. https://www.fao.org/documents/card/en/c/cb3673en/

[90] https://blogs.worldbank.org/opendata/updated-estimates-impact-covid-19-global-poverty-turning-corner-pandemic-2021

[91] The State of Food Security and Nutrition in the World 2021. Rome, FAO. Transforming food systems for food security, improved nutrition, and affordable healthy diets for all. https://docs.wfp.org/api/documents/WFP-0000130141/download/?_ga=2.47516911.931354890.1634299853-763856357.1633873374

[92] GRFC. 2021. Global Report on Food Crises: Joint Analysis for Better Decisions. September 2021 Update. http://www.fightfoodcrises.net/fileadmin/user_upload/fightfoodcrises/doc/resources/FINAl_GRFC2021_Sept_Update.pdf

rates remained at modest levels in 2021, buffered by subsidies on many basic commodities that prevented price increase.

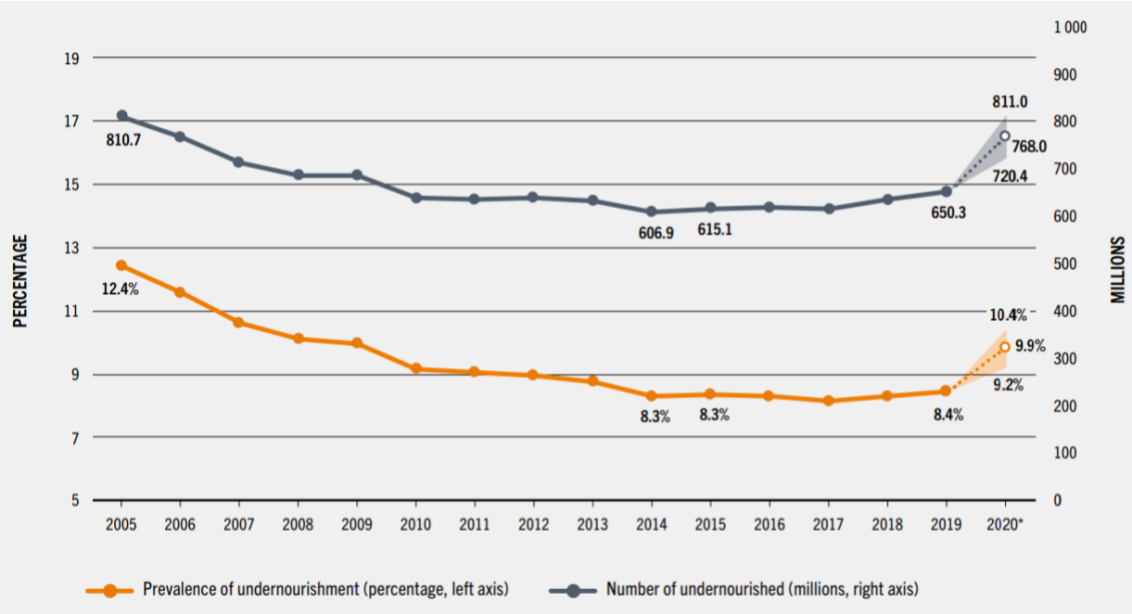

Figure 25: The number of undernourished people in the world significantly increased during the COVID-19 pandemic, from 650 million people in 2019 to 768 million people in 2020. Dotted lines and empty circles illustrate projected values in the above figure. According to the 2021 State of Food Security and Nutrition in the World, projections show a decrease in undernourishment rates between 2021 and 2030, with divergent trends across regions. While the numbers of undernourished people are likely to decrease in Asia, from 418 million in 2020 to ≈295 million in 2030, in Africa, the projected number of undernourished people is likely to increase, from 282 million in 2020 to ≈290 million in 2030. The entire series was revised to reflect new information made available since the publication of the report (GRFC, 2021).

Impacts of weather hazards on food production

Extreme weather during the 2020/21 La Niña altered rainfall seasons, disrupting livelihoods and agricultural campaigns across the world. Extreme weather events during the 2021 rainfall season have compounded shocks from the previous year(s), making it increasingly difficult to quantify impacts resulting from one single event. Consecutive droughts across large parts of Africa, Asia, and Latin America have coincided with severe storms, cyclones and hurricanes, significantly affecting livelihoods and the ability to recover from recurrent weather shocks.

Extreme dry conditions across vast areas of South America, and the recent return of La Niña conditions could further threaten crop yields within this region. However, larger than usual cultivations have to some extent offset the adverse effects of La Niña-induced crop productivity losses throughout the continent (-3.6% in 2021 compared to 2020)[93]. In the Caribbean, Haiti has been triply hit by natural disasters (earthquakes), weather shocks (irregular rains) and political instability, increasing agricultural damage and significantly worsening food insecurity.

In West Africa, floods and dry spells have caused crop damage and losses in localized areas resulting in small production downturns in 2021, but the forecasted aggregate outputs for the whole continent remain above average (+2.9% in 2021 over 2020)[93]. The 2021 first season harvest along central and southern areas of East Africa has been negatively affected by prolonged droughts, mostly in Kenya where maize outputs have been officially estimated to be 42-70% below average[93]. In northern parts of East Africa, the scale of seasonal flooding and its impact on crops has been lower compared to the severe flood impacts in 2020. In Southern Africa, the second consecutive

[93] FAO. 2021. Crop prospects and food situation. Quarterly Global report. https://www.fao.org/3/cb6901en/cb6901en.pdf

below-average rainfall season in Madagascar has led to a severe reduction in staple food production and a decline in livestock herd size. Although rainfall is projected to be near average in Madagascar in autumn 2021, seed and cutting supplies will be insufficient for the next cropping season and the lack of government and household control of weather-related hazards, pests and diseases, will result in sharp harvest declines with yield estimates 50-70% below the five-year average[94]. In Mozambique, cyclone Eloise made landfall in late January during the region's lean season when vulnerabilities were at their highest and affected communities still recovering from Cyclone Idai barely two years ago. According to the Government of Mozambique more than 441 000 people were affected by the cyclone displacing nearly 44 000 and destroying more than 45 000 hectares of cropland[95].

Drought conditions in the Near East reduced cereal production to below-average levels, exacerbating the impacts on agriculture and food security in fragile contexts, mostly in Afghanistan and the Syrian Republic. While cereal production decreased in the Near East, wheat production in the Far East reached a record high in 2021, with paddy rice outputs at high levels due to suitable weather conditions. In contrast, Central China was hit by torrential rains in mid-July 2021, leading to significant loss of life and damage to property. This sparked concerns over the potential impact on the nation's food supplies, as 1 million hectares of cropland – mostly corn, soybeans and peanuts – were affected, a third of which were wiped out.

Population Displacement

Climate-related hazards were a major driver of new displacement

Extreme weather events and conditions have had major and diverse impacts on population displacement and on the vulnerability of people already displaced throughout the year. From Afghanistan to Central America, droughts, flooding and other extreme weather events are hitting those least equipped to recover and adapt[96]. Similar to previous years, many of the largest scale displacements in 2021 occurred in populous Asian countries. Most disaster displacements in 2021 resulted from tropical storms and floods in East Asia and the Pacific, South Asia, the Americas and Sub-Saharan Africa.

Over the course of 2021, hazardous weather events and environmental degradation have further contributed to the displacement of millions more people in exposed and vulnerable situations. This includes the impact of rapid-onset events such as floods, storms and wildfires, as well as slow-onset processes such as drought and desertification, affecting people's safety and ability to meet their basic needs for survival such as food, water, resilient housing and productive land. Over the first half of the year in Afghanistan, for example, disasters brought on some 22 500 new displacements, primarily linked to floods[97]. In June, the government declared a national drought with 80% of the country classified as being in either severe or serious drought status on top of escalating conflict, food insecurity and health and socio-economic impacts of COVID-19 and with humanitarian, development and government actors foreseeing that agricultural families would very likely become displaced[98]. People forced to leave their homes had to sell their assets and engage in dangerous work to survive, while some children were sent to work in other areas or in neighbouring countries or were married off as a way to reduce financial burdens[99].

---

[94] FEWSNET. 2021. *Madagascar Food Security Alert: June 10, 2021* *https://reliefweb.int/sites/reliefweb.int/files/resources/Madagascar%20Food%20Security%20Alert%20-%20June%2010%2C%202021.pdf*

[95] https://www.fao.org/mozambique/news/detail-events/en/c/1393190/

[96] UNHCR News Stories April 2021 : https://www.unhcr.org/news/stories/2021/4/60806d124/data-reveals-impacts-climate-emergency-displacement.html

[97] IDMC 2021 Mid-Year Update. https://story.internal-displacement.org/2021-midyear-review/index.html

[98] DRC https://prod.drc.ngo/about-us/for-the-media/press-releases/2021/7/drought-crisis-in-afghanistan-intensifies-risk-of-displacement/

[99] Ibid.

In line with established trends, 2021 saw the overwhelming majority of new displacements related to hazardous weather events take place within national borders. Most of these internal displacements were triggered by typhoons, floods, earthquakes and volcanic eruptions, especially in the East Asia and Pacific region. The countries with the highest numbers of displacements recorded as of October 2021 were China (more than 1.4 million evacuations recorded in July 2021), the Philippines (more than 214,000 in July and more than 386,000 in October) and Vietnam (more than 664,000 displacements recorded in September 2021)[100].

High-income countries were also affected. In the western parts of the United States and Canada exceptional heatwaves, drought, and wildfires displaced thousands from their homes. Wildfires also compounded risks related to other hazards, further increasing the risk of displacement. For instance, 15 000 people were displaced in California in January 2021, following mandatory pre-emptive evacuation orders following heavy rains[101].

Hydro-meteorological hazards fuelled patterns of protracted, prolonged and repeated displacement

Many displacement situations triggered by hydro-meteorological events have become prolonged or protracted for people unable to return to their former homes or without options for integrating locally or settling elsewhere. As of the beginning of 2021, at least 7 million people were living in internal displacement following disasters[102] related to natural hazard events in previous years (IDMC, Internal Displacement Monitoring Centre). The highest numbers of these people were in Afghanistan, India and Pakistan, followed by Ethiopia, Sudan, Bangladesh, Niger and Yemen[103].

Due to continuing or growing risk in their areas of origin (and return) or settlement, people who have been displaced by hydro-meteorological and climatic events may also be subject to repeated and frequent displacement, leaving little time for recovery between one shock and the next. In Indonesia, for example, 557 000 new disaster displacements were recorded in the first half of the year, mostly triggered by major rainy season floods. Human activities, including deforestation, urbanisation and land degradation have reduced the capacity of some regions of Indonesia to absorb heavy rainfall. With heavy rainfall during La Niña, the floods triggered an estimated 190 000 new displacements in the Kalimantan province in January and 161 000 new displacements on the island of Java in February. Further displacements are expected to arise during the new rainy season, starting from November 2021[104]. Such situations highlight the importance of disaster preparedness and risk management, but also for supporting solutions to displacement that are sustainable and supporting the resilience of people who might otherwise see their living conditions progressively eroded through repeated disasters and displacement.

Hazardous weather events and changing climatic conditions also added to the multiple risks faced by internally displaced people in conflict-affected countries and refugees

In Yemen, for instance, the annual rainy season brings heavy rainfall, high winds and flooding, particularly to coastal areas. In mid-April heavy rain and flooding hit several parts of the country affecting 7 000 people, 75% of whom were internally displaced people living in precarious conditions[105] It has also contributed to population displacement in what is already the world's fourth

[100] Data sourced from the Internal Displacement Monitoring Centre's Updates: https://www.internal-displacement.org/global-displacement-map
[101] IDMC 2021 Mid-Year Update. https://story.internal-displacement.org/2021-midyear-review/index.html
[102] IDMC 2021, GRID Report, Data as of 31 December 2020.
[103] Data sourced from the Internal Displacement Monitoring Centre's Updates, 2021: https://www.internal-displacement.org/global-displacement-map
[104] IDMC 2021 Mid-Year Update. https://story.internal-displacement.org/2021-midyear-review/index.html
[105] UNOCHA Humanitarian Update, Yemen, Issue 5, May 2021

biggest internal displacement crisis, with over 4 million internally displaced people. The annual rainy season brings heavy rainfalls, high winds and flooding, particularly to coastal areas, with thousands of families already impacted by flash floods in 2021. By blocking passage of roads, flooding also continues to impede the ability of humanitarian partners to deliver lifesaving assistance to people in need[106].

In Mozambique, multiple tropical storms and floods, on top of recurrent disease outbreaks and conflict[107], significantly increased the vulnerability of people affected[108], including thousands of families still displaced since Cyclones Idai and Kenneth in 2019. In January, strong winds and floods from Tropical Storm Chalane and then Cyclone Eloise damaged or destroyed the shelters of over 8 700 of these internally displaced families as well as schools and hospitals[109]. These events also resulted in new displacement, with Cyclone Eloise displacing more than 43 300 people[110]. Greater attention is needed to reduce climate vulnerability and risks in fragile and conflict-affected contexts and strengthen community-based preparedness[111].

In East Africa, floods and droughts resulted in large-scale displacement, especially in Somalia and Ethiopia, many of whom were people already living in overcrowded and insecure camps for internally displaced people to which many newly flood-displaced people also moved. Farmers whose crops were devastated by desert locusts were also forced to move in search of survival assistance[112].

Nigeria also experienced drought and floods, which affected agricultural activities, resulting in loss of shelter and increased vulnerability of people already displaced by conflict in the northeast. The situation further deteriorated in the first half of 2021, with around 294 000 new displacements reported between January and June 2021[113].

In Bangladesh, monsoon rains led to massive flooding and the displacement of millions of people following Cyclone Yaas in June 2021. In the Rohingya refugee sites in Cox's Bazar, over 6 000 shelters were damaged and more than 25 000 refugees were forced to seek shelter in communal facilities or with other families[114]. Without preparedness measures undertaken in the camp areas, including the strengthening of shelters, the building of retaining structures on hillsides and improved drainage, roads and bridges, these impacts would have been far worse.

Climate impacts on ecosystems

Ecosystems – including terrestrial, freshwater, coastal and marine ecosystems – and the services they provide, are affected by the changing climate and some are more vulnerable than others[115]. In addition, ecosystems are degrading at an unprecedented rate. The degradation of ecosystems is

[106] Relief Web, Yemen August 2021, https://reliefweb.int/report/yemen/climate-crisis-exacerbates-humanitarian-situation-yemen-enar

[107] UNHCR 2021: https://www.unhcr.org/news/briefing/2021/4/606c17bf4/unhcr-scales-response-thousands-flee-attacks-northern-mozambique.html

[108] UNHCR News Mozambique April 2021 https://www.unhcr.org/news/briefing/2021/4/606c17bf4/unhcr-scales-response-thousands-flee-attacks-northern-mozambique.html

[109] IOM/DTM Mozambique Flash Report 16- Cyclone Eloise (January 2021) https://displacement.iom.int/reports/mozambique-%E2%80%93-flash-report-16-tropical-cyclone-eloise-january-2021?close=true

[110] https://reliefweb.int/report/afghanistan/internal-displacement-mid-year-10-situations-review

[111] Ibid

[112] UNHCR News Somalia August 2021, https://www.unhcr.org/news/stories/2021/8/611a2bca4/displaced-somalis-refugees-struggle-recover-climate-change-brings-new-threats.html

[113] Ibid

[114] UNHCR, News Bangladesh July 2021 https://www.unhcr.org/news/stories/2021/7/6103c43c4/floods-bring-new-misery-rohingya-refugees-bangladesh-camps.html

[115] United Nations Environment Programme (2021). Adaptation Gap Report 2020. Nairobi.

limiting their ability to support human well-being and harming their adaptive capacity to build resilience[116].

For example, mountain ecosystems – the water towers of the world – are vulnerable and can be profoundly affected by climate change due to their low capacity to adapt. This may affect the 1.9 million people living in mountain areas[117]. Climate change may exacerbate water stress, especially in areas of decreased precipitation and where groundwater is already being depleted, affecting agricultural production, arable land, and the more than 2 billion people who are already experiencing water stress[116].

Climate change is also affecting temperature-sensitive plants and other species. There is evidence that temperature-sensitive plants are leafing out and flowering earlier in spring and dropping their leaves later in autumn. Also, there has been a clear shift in the timing of marine and freshwater fish spawning events and animal migrations worldwide. Substantial changes in species' abundance and distribution may in turn affect the interactions between species[118]. Climate change also exacerbates other threats to biodiversity. The number of species projected to go extinct increases dramatically as global temperatures rise – and is 30% higher at 2 °C warming than at 1.5 °C warming[116].

Meanwhile, large-scale changes have been observed in marine ecosystems, including declining ocean productivity, migration of species to higher latitudes, and damage to coral reefs and mangroves. Warming towards 1.5 °C will increase water temperatures and change the ocean's chemistry (e.g., acidification), resulting in new ecosystems. Species that are less able to relocate are projected to experience high rates of mortality and loss[119]. Climate change is also triggering the disintegration of the Greenland and Antarctic ice sheets and increasing the chances of the Arctic Ocean being ice-free in the summer, further disrupting ocean circulation and Arctic ecosystems[116].

Rising temperatures heighten the risk of irreversible loss of marine and coastal ecosystems, including seagrass meadows and kelp forest. Coral reefs are especially vulnerable to climate change. They are projected to lose between 70 and 90% of their former coverage area at 1.5 °C of warming and over 99% at 2 °C. Between 20 and 90% of current coastal wetlands are at risk of being lost by the end of this century, depending on how fast sea levels rise. This will further compromise food provision, tourism, and coastal protection, among other ecosystem services[116].

[116] United Nations Environment Programme (2021). Making Peace with Nature: A scientific blueprint to tackle the climate, biodiversity and pollution emergencies. Nairobi.
[117] Immerzeel, W.W., Lutz, A.F., Andrade, M., Bahl, A., Biemans, H., Bolch, T. et al. (2020). Importance and vulnerability of the world's water towers. Nature 577, 364-369. https://doi.org/10.1038/s41586-019-1822-y.
[118] Scheffers, B.R., De Meester, L., Bridge, T.C., Hoffmann, A.A., Pandolfi, J.M., Corlett, R.T. et al. (2016). The broad footprint of climate change from genes to biomes to people. Science 354(6313), aaf7671. https://doi.org/10.1126/science.aaf7671.
[119] Intergovernmental Panel on Climate Change (IPCC) (2018). Summary for policymakers. In Global Warming of 1.5°C: An IPCC Special Report on the Impacts of Global Warming of 1.5°C above Pre-industrial Levels and Related Global Greenhouse Gas Emission Pathways, in the Context of Strengthening the Global Response to the Threat of Climate Change, Sustainable Development, and Efforts to Eradicate Poverty. Masson-Delmotte, V., Zhai, P., Pörtner, H.-O., Roberts, D., Skea, J., Shukla, J.R. et al. (eds.). Cambridge: Cambridge University Press.

Contributors

WMO Members

Algeria, Andorra, Argentina, Armenia, Australia, Austria, Bahrain, Belarus, Bosnia and Herzegovina, Bulgaria, Burkina Faso, Cameroon, Canada, Chile, China, Colombia, Croatia, Cyprus, Czech Republic, Denmark, Estonia, Finland, France, Georgia, Germany, Greece, Guinea, Guinea Bissau, Hungary, India, Iran, Ireland, Israel, Italy, Japan, Jordan, Kazakhstan, Kenya, Latvia, Libya, Lithuania, Luxembourg, Macao China, Madagascar, Mali, Mauritius, Moldova, Morocco, New Zealand, Niger, Nigeria, North Macedonia, Norway, Pakistan, Peru, Poland, Portugal, Romania, Russian Federation, Saudi Arabia, Senegal, Serbia, Slovakia, Slovenia, South Africa, Spain, Sweden, Switzerland, Syria, Tanzania, Thailand, The Netherlands, Togo, Trinidad and Tobago, Tunisia, Turkey, Ukraine, United Kingdom, United States, Uruguay, Uzbekistan.

Institutional contributors

ARC Centre of Excellence for Climate Extremes, University of Tasmania; British Antarctic Survey (BAS); Bureau of Meteorology (BoM); Carbon Portal, Lund University; Centre National d'Études Spatiales, CNES, France; Mercator Ocean international, France; Observatoire Midi-Pyrénées, France; IFREMER, France; University of Brest, France; Centre National de la Recherche Scientifique, (CNRS), France; Institut de Recherche pour le Développement (IRD), France; Laboratoire d'Océanographie Physique et Spatiale (LOPS), France; Laboratoire d'Etudes en Géophysique et Océanographie Spatiales (LEGOS), France; Institut Universitaire Européen de la Mer (IUEM), France; CELAD, France; Sorbonne Université, France; Laboratoire d'Océanographie de Villefranche, France; Center for Ocean Mega-Science, Chinese Academy of Sciences; Copernicus Climate Change Service (C3S); CSIRO Oceans and Atmosphere; Danmarks Meteorologiske Institut (DMI); Global Precipitation Climatology Centre, Deutscher Wetterdienst (GPCC, DWD); Environment and Climate Change Canada (ECCC); ETH Zürich; European Centre for Medium Range Weather Forecasts (ECMWF); Food and Agriculture Organisation (FAO); George Washington University; Hong Kong Observatory; Ifremer; Institute of Atmospheric Physics, Chinese Academy of Sciences (IAP, CAS); Intergovernmental Oceanographic Commission of the United Nations Educational, Scientific and Cultural Organization (IOC UNESCO); Japan Marine-Earth Science and Technology (JAMSTEC); Joint Institute for Marine and Atmospheric Research, University of Hawai'i (JIMAR); Laboratory of Space Geophysical and Oceanographic Studies (LEGOS); Mercator Ocean International; Met Office Hadley Centre; Meteorological Research Institute, Department of Atmosphere, Ocean and Earth System Modeling Research; National Oceanographic and Atmosphere Administration, National Centers for Environmental Information (NOAA NCEI); NOAA, Pacific Marine Environmental Laboratory (NOAA PMEL); National Oceanography Centre (NOC); Natural Resources Canada; Norwegian Meteorological Institute; Rutgers University; Scripps Institution of Oceanography; Tokyo Climate Center, Japan Meteorological Agency (TCC, JMA); United Nations Environment Programme (UNEP); United Nations High Commissioner for Refugees (UNHCR); United Nations Office for Disaster Risk Reduction (UNDRR); Universidade Federal do Rio de Janeiro; University of Exeter; Woods Hole Oceanographic Institution; World Climate Research Programme (WCRP); World Data Centre for Greenhouse Gases (WDCGG); World Food Programme (WFP)

Individual contributors

Signe Aaboe (Norwegian Meteorological Institute), Jorge Alvar-Beltrán (FAO), Omar Baddour (WMO), Jessica Blunden (NOAA NCEI), Tim Boyer (NOAA NCEI), Anny Cazenave (LEGOS CNES and OMP), Lijing Cheng (IAP; Center for Ocean Mega-Science, Chinese Academy of Sciences), Louis Clement (National Oceanography Centre), Damien Desbruyères (Ifremer, CNRS, IRD, Laboratoire d'Océanographie Physique et Spatiale), Catia Domingues (NOC; ARC Centre of Excellence for Climate

Extremes, University of Tasmania), Robert Dunn (Met Office Hadley Centre), Thomas Estilow (Rutgers University), Florence Geoffroy (UNHCR), Nathan Gillett (ECCC), John Gilson (University of California), Loretta Hieber Girardet (UNDRR), Atsushi Goto (TCC, JMA), Yvan Gouzenes (LEGOS and OMP), Stephan Gruber, (Carleton University), Ana Heureux (FAO), Shigeki Hosoda (JAMSTEC), Matthias Huss (ETH Zürich), Kirsten Isensee (IOC UNESCO), Masayoshi Ishii (Meteorological Research Institute, Department of Atmosphere, Ocean and Earth System Modeling Research), Gregory C. Johnson (NOAA, PMEL), Maarten Kappelle (UNEP), John Kennedy (Met Office Hadley Centre), Rachel Killick (Met Office Hadley Centre), Brian A. King (NOC), Nicolas Kolodziejczyk (University of Brest, CNRS, IRD, Ifremer, Laboratoire d'Océanographie Physique et Spatiale, IUEM), Animesh Kumar (UNDRR), Gernot Laganda (WFP), Thomas Lavergne (Norwegian Meteorological Institute), Renata Libonati (Universidade Federal do Rio de Janeiro), John Lyman (NOAA, Pacific Marine Environmental Laboratory; JIMAR, University of Hawaii), Shawn Marshall (Environment and Climate Change Canada and University of Calgary), Jesse Mason (WFP), Brian Menounos (University of Northern British Columbia), Maeva Monier (CELAD/Mercator Ocean International), Lev Neretin (FAO), Didier Paolo Monselesan (Scripps Institution of Oceanography, University of California San Diego), Colin Morice (Met Office Hadley Centre), Stoyka Netcheva (WMO), Rodica Nitu (WMO), Jeannette Noetzli, (Institute for Snow and Avalanche Research), Ben Pelto (University of Northern British Columbia), David Robinson (Rutgers University), Dean Roemmich (CSIRO Oceans and Atmosphere), Kanako Sato (JAMSTEC: Japan Marine-Earth Science and Technology), Yousuke Sawa (Japan Meteorological Agency, WDCGG), Robert W. Schlegel (Sorbonne Université, CNRS, Laboratoire d'Océanographie de Villefranche), Katherina Schoo (IOC UNESCO), Karina von Schuckmann (Mercator Ocean international), Rahul Sengupta (UNDRR), Fumi Sezaki (TCC, JMA), Sharon Smith, (Natural Resources Canada), Michael Sparrow (WCRP), Martin Stendel (DMI), Peter Stott (Met Office Hadley Centre, University of Exeter), Dmitry Streletskiy, (George Washington University), Toshio Suga (JAMSTEC: Japan Marine-Earth Science and Technology; Tohoku University), Oksana Tarasova (WMO), Blair Trewin (Bureau of Meteorology), John Turner (BAS), Freja Vamborg (ECMWF), Alex Vermeulen (Carbon Portal, Lund University), Ying Wang (UNEP), Susan E. Wijffels (Scripps Institution of Oceanography; Woods Hole Oceanographic Institution), Michelle Yonetani (UNHCR), Markus Ziese (DWD).

Data sets and methods

Greenhouse gas data

Estimated concentration from 1750 are used to represent pre-industrial conditions. Calculations assume a pre-industrial mole fraction of 278 ppm for CO_2, 722 ppb for CH_4 and 270 ppb for N_2O.

WMO Greenhouse Gas Bulletin, No.17, October 2021,
https://library.wmo.int/index.php?lvl=notice_display&id=21975

World Data Centre for Greenhouse Gases operated by Japan Meteorological Agency
https://gaw.kishou.go.jp/

World Ozone and Ultraviolet Radiation Data Centre operated by Environment and Climate Change Canada

https://woudc.org/home.php

Global Temperature data

Six data sets are used in the calculation of global temperature. Global mean temperature anomalies are calculated relative to an 1850 to 1900 baseline using the following steps

1. For each data set, anomalies are calculated relative to the 1981-2010 average
2. 0.69 °C was added to each series, based on the estimated difference between 1850-1900 and 1981-2010 calculated using the method from IPCC AR6 WG1 (see caption for Figure 1.12).
3. The mean and standard deviation of the six estimates were calculated.
4. The uncertainty in the IPCC estimate was combined with the standard deviation assuming the two are independent and assuming the IPCC uncertainty range (0.54 to 0.78 °C) is representative of a 90% confidence range (1.645 standard deviations).

The following six data sets used were:

HadCRUT.5.0.1.0 —Morice, C.P. et al., 2021. An Updated Assessment of Near-Surface Temperature Change From 1850: The HadCRUT5 Data Set. Journal of Geophysical Research: Atmospheres, 126(3): e2019JD032361. doi: https://doi.org/10.1029/2019JD032361. HadCRUT.5.0.1.0 data were obtained from http://www.metoffice.gov.uk/hadobs/hadcrut5 on 24 October 2021 and are © British Crown Copyright, Met Office 2021, provided under an Open Government License, http://www.nationalarchives.gov.uk/doc/open-government-licence/version/3/.

NOAAGlobalTemp v5 — Zhang, H.-M., et al., NOAA Global Surface Temperature Dataset (NOAAGlobalTemp), Version 5.0. NOAA National Centers for Environmental Information. doi:10.7289/V5FN144H, https://www.ncei.noaa.gov/access/metadata/landing-page/bin/iso?id=gov.noaa.ncdc:C00934. Huang, B. et al., 2020: Uncertainty Estimates for Sea Surface Temperature and Land Surface Air Temperature in NOAAGlobalTemp Version 5. Journal of Climate 33(4): 1351–1379, https://journals.ametsoc.org/view/journals/clim/33/4/jcli-d-19-0395.1.xml.

GISTEMP v4 — GISTEMP Team, 2019: GISS Surface Temperature Analysis (GISTEMP), version 4. NASA Goddard Institute for Space Studies, https://data.giss.nasa.gov/gistemp/. Lenssen, N.J.L. et al., 2019: Improvements in the GISTEMP Uncertainty Model. Journal of Geophysical Research: Atmospheres 124(12): 6307–6326, doi: https://doi.org/10.1029/2018JD029522.

Berkeley Earth – Rohde, R. A. and Hausfather, Z.: The Berkeley Earth Land/Ocean Temperature Record, Earth Syst. Sci. Data, 12, 3469–3479, https://doi.org/10.5194/essd-12-3469-2020, 2020.

ERA5 — Hersbach, H. et al., 2020 : The ERA5 Global Reanalysis. Quarterly Journal of the Royal Meteorological Society 146(730): 1999–2049, doi: https://doi.org/10.1002/qj.3803.

JRA-55 — Kobayashi, S. et al., 2015: The JRA-55 Reanalysis: General Specifications and Basic Characteristics. Journal of the Meteorological Society of Japan. Ser. II 93(1): 5–48, doi:10.2151/jmsj.2015-001, https://www.jstage.jst.go.jp/article/jmsj/93/1/93_2015-001/_article.

Ocean heat content data

Hosoda, S. et al., 2008: A Monthly Mean Dataset of Global Oceanic Temperature and Salinity Derived from Argo Float Observations. JAMSTEC Report of Research and Development, 8: 47–59, doi: https://www.jstage.jst.go.jp/article/jamstecr/8/0/8_0_47/_article.

JAMSTEC,

CARS2009 (http://www.marine.csiro.au/~dunn/cars2009/),

Roemmich, D. and J. Gilson. 2009: The 2004–2008 Mean and Annual Cycle of Temperature, Salinity, and Steric Height in the Global Ocean from the Argo Program. Progress in Oceanography, 82(2): 81–100, https://www.sciencedirect.com/science/article/abs/pii/S0079661109000160?via%3Dihub.

Copernicus Marine Ocean Monitoring Indicators (http://marine.copernicus.eu/science-learning/ocean-monitoring-indicators; CORA);

Good, S.A. et al., 2013: EN4: Quality Controlled Ocean Temperature and Salinity Profiles and Monthly Objective Analyses with Uncertainty Estimates. Journal of Geophysical Research: Oceans 118(12): 6704–6716, doi: https://agupubs.onlinelibrary.wiley.com/doi/ full/10.1002/2013JC009067.

Desbruyères, D.G. et al., 2016: Deep and Abyssal Ocean Warming from 35 Years of Repeat Hydrography. Geophysical Research Letters 43(19): 10,356-10,365, doi: https://doi.org/10.1002/2016GL070413 .

Sea level data

GMSL from CNES/Aviso+ https://www.aviso.altimetry.fr/en/data/products/ocean-indicators-products/mean-sea-level/data-acces.html#c12195

Marine heatwave and marine cold spell data

MHWs are categorized as moderate when the sea-surface temperature (SST) is above the 90th percentile of the climatological distribution for five days or longer; the subsequent categories are defined with respect to the difference between the SST and the climatological distribution average: strong, severe, or extreme, if that difference is, respectively, more than two, three or four times the difference between the 90th percentile and the climatological distribution average (Hobday et al., 2018). MCS categories are analogous but counting days below the 10th percentile.

The baseline used for MHWs and MCSs is 1982–2011, which is shifted by one year from the standard normal period of 1981–2010 because the first full year of the satellite SST series on which it is based is 1982.

Hobday, A.J. et al., 2018: Categorizing and Naming Marine Heatwaves. Oceanography, 31(2): 1–13. doi: https://eprints.utas.edu.au/27875/.

NOAA OISST v2: Optimum Interpolation Sea Surface Temperature (OISST):

Banzon, V. et al., 2016: A Long-Term Record of Blended Satellite and in Situ Sea-Surface Temperature for Climate Monitoring, Modeling and Environmental Studies. Earth System

Science Data, 8(1): 165–176. doi: https://essd.copernicus.org/articles/8/165/2016/.

Greenland ice sheet data

Changes in surface mass balance and total mass balance are based on the average of three regional climate and mass balance models. See Mankoff, K. D., X. Fettweis, P.L. Langen, M. Stendel, K.K. Kjeldsen, N.B. Karlsson, B. Noël, M.R. van den Broeke, W. Colgan, S.B. Simonsen, J.E. Box, A. Solgaard, A.P. Ahlstrøm, S.B. Andersen and R.S. Fausto, 2021: Greenland ice sheet mass balance from 1840 through next week. Earth Syst. Sci. Data, https://doi.org/10.5194/essd-2021-131, accepted.

The melt season is defined as the first of at least three days in a row with melting over at least 5% of the area of the ice sheet.

Ablation is defined as the first of at least three days in a row with a negative surface mass balance of at least -1 Gt.

Snow data

Snow data and monthly anomaly timeseries charts are available at:

https://climate.rutgers.edu/snowcover/files/wmo/rutgers-nh-sce-anomalies-2020-21-data.xlsx

Sea ice data

Data set background: The sea ice section uses data from the EUMETSAT OSI SAF Sea Ice Index v2.1 (OSI-SAF, based on Lavergne et al., 2019) and the NSIDC v3 Sea Ice Index (Fetterer et al., 2017). Sea ice concentrations are estimated from microwave radiances measured from satellites. Extent is calculated as the area of ocean grid cells where the sea-ice concentration exceeds 15%. Although there are relatively large differences in the absolute extent between data sets, they agree well on the year-to-year changes and the trends. In this report, NSIDC are reported for absolute extents (e.g. "18.95 million km2") for consistency with earlier reports, while rankings are reported for both data sets.

Fetterer, F., K. Knowles, W. N. Meier, M. Savoie, and A. K. Windnagel. 2017, updated daily. Sea Ice Index, Version 3. Boulder, Colorado USA. NSIDC: National Snow and Ice Data Center. doi: https://doi.org/10.7265/N5K072F8. Accessed Oct. 2021.

EUMETSAT Ocean and Sea Ice Satellite Application Facility, Sea ice index 1979-onwards (v2.1, 2020), OSI-420, Data extracted from OSI SAF FTP server: 1979-2020, Northern and Southern Hemisphere, accessed Oct. 2021.

Lavergne, T., Sørensen, A. M., Kern, S., Tonboe, R., Notz, D., Aaboe, S., Bell, L., Dybkjær, G., Eastwood, S., Gabarro, C., Heygster, G., Killie, A., Brandt Kreiner, M., Lavelle, J., Saldo, R., Sandven, S., and Pedersen, L. T.: Version 2 of the EUMETSAT OSI SAF and ESA CCI sea-ice concentration climate data records, The Cryosphere, 13, 49–78, https://doi.org/10.5194/tc-13-49-2019, 2019.

Permafrost data

Noetzli, J., Christiansen, H.H., Hrbáček, F., Isaksen, K., Smith, S. L., Zhao, L., and Streletskiy, D.A. (2021) [Global Climate] Permafrost Thermal State [in State of the Climate in 2020]. Bulletin of the American Meteorological Society, 102 (8): S42-S44. doi:10.1175/BAMS-D-21-0098.1

Smith, S.L., Romanovsky, V.E., Isaksen, K., Nyland, K.E., Kholodov, A.L., Shiklomanov, N.I., Streletskiy, D.A., Farquharson, L.M., Drozdov, D.S., Malkova, G.V., and Christiansen, H.H. (2021) [Arctic] Permafrost [in State of the Climate in 2020]. Bulletin of the American Meteorological Society, 102 (8): S293-S297. doi:10.1175/BAMS-D-21-0086.1

Precipitation data

These GPCC data sets were used in the analysis:

- First Guess Monthly, DOI: 10.5676/DWD_GPCC/FG_M_100
- Monitoring Product (Version 2020), DOI: 10.5676/DWD_GPCC/MP_M_V2020_100
- Full Data Monthly (Version 2020), DOI: 10.5676/DWD_GPCC/FD_M_V2020_100
- First Guess Daily, DOI: 10.5676/DWD_GPCC/FG_D_100
- Full Data Daily (Version 2020), DOI: 10.5676/DWD_GPCC/FD_D_V2020_100

Indian Monsoon: https://mausam.imd.gov.in/imd_latest/contents/monsoon.php